An Integrated Genomics Approach to Define Niche Establishment by *Rhodococcus fascians*[1][C][W][OA]

Stephen Depuydt, Sandra Trenkamp, Alisdair R. Fernie, Samira Elftieh, Jean-Pierre Renou, Marnik Vuylsteke, Marcelle Holsters*, and Danny Vereecke

Department of Plant Systems Biology, Flanders Institute for Biotechnology, 9052 Ghent, Belgium (S.D., M.V., M.H., D.V.); Department of Plant Biotechnology and Genetics, Ghent University, 9052 Ghent, Belgium (S.D., M.V., M.H., D.V.); Max Planck Institute of Molecular Plant Physiology, University of Potsdam, 14476 Potsdam-Golm, Germany (S.T., A.R.F.); and Unité Mixte de Recherche en Génomique Végétale, Institut National de la Recherche Agronomique, 91057 Evry, France (S.E., J.-P.R.)

Rhodococcus fascians is a Gram-positive phytopathogen that induces shooty hyperplasia on its hosts through the secretion of cytokinins. Global transcriptomics using microarrays combined with profiling of primary metabolites on infected Arabidopsis (*Arabidopsis thaliana*) plants revealed that this actinomycete modulated pathways to convert its host into a niche. The transcript data demonstrated that *R. fascians* leaves a very characteristic mark on Arabidopsis with a pronounced cytokinin response illustrated by the activation of cytokinin perception, signal transduction, and homeostasis. The microarray data further suggested active suppression of an oxidative burst during the *R. fascians* pathology, and comparison with publicly available transcript data sets implied a central role for auxin in the prevention of plant defense activation. Gene Ontology categorization of the differentially expressed genes hinted at a significant impact of infection on the primary metabolism of the host, which was confirmed by subsequent metabolite profiling. The much higher levels of sugars and amino acids in infected plants are presumably accessed by the bacteria as carbon and nitrogen sources to support epiphytic and endophytic colonization. Hexoses, accumulating from a significantly increased invertase activity, possibly inhibited the expression of photosynthesis genes and photosynthetic activity in infected leaves. Altogether, these changes are indicative of sink development in symptomatic tissues. The metabolomics data furthermore point to the possible occurrence of secondary signaling during the interaction, which might contribute to symptom development. These data are placed in the context of regulation of bacterial virulence gene expression, suppression of defense, infection phenotype, and niche establishment.

Plants have evolved a remarkable level of developmental plasticity enabling them to deal with changes in their immediate surroundings throughout their life cycle. Environmental stress affects plants in their growth and development by imposing alterations in gene expression and, consequently, in physiology and metabolism. Pathogenic bacteria, fungi, viruses, oomycetes, nematodes, and insects can have a devastating effect on crop plants either at the survival or the yield level. Although the dynamic interaction between pathogen and host is complex and, at first sight, seemingly specific for each plant-pathogen combination, several biotrophic phytopathogens display related mechanisms to convert the plant into a suitable niche (Jameson, 2000).

In contrast to necrotrophic pathogens, biotrophs rely on living tissues for survival and multiplication. To exploit the plant as a source of energy and assimilates, the first requirement is to avoid preformed and suppress induced defense mechanisms of the host. Typical defense responses include cell wall strengthening, production of phytoalexins and proteins with antimicrobial properties, and synthesis of stress signaling molecules, such as salicylic acid, jasmonic acid, ethylene, and reactive oxygen species (ROS; Hammond-Kosack and Jones, 1996; Gadjev et al., 2006; Garcia-Brugger et al., 2006; Berger et al., 2007). Bacterial effector molecules have been proposed to suppress or delay defense and, in Gram-negative pathogenic bacteria, are typically secreted via the type III secretion system (Biemelt and Sonnewald, 2006; Jones and Dangl, 2006; Truman et al., 2006). In the next phase toward successful niche establishment, plant (carbohydrate) metabolism is diverted for bacterial nutrition. Indeed, pathogens have proven to be very effective sinks for

[1] This work was supported by the Bijzonder Onderzoeksfonds of Ghent University and the European Molecular Biology Organization (predoctoral and short-term fellowships, respectively, to S.D.).

* Corresponding author; e-mail marcelle.holsters@psb.ugent.be.

The author responsible for distribution of materials integral to the findings presented in this article in accordance with the policy described in the Instructions for Authors (www.plantphysiol.org) is: Danny Vereecke (danny.vereecke@psb.ugent.be).

[C] Some figures in this article are displayed in color online but in black and white in the print edition.

[W] The online version of this article contains Web-only data.

[OA] Open Access articles can be viewed online without a subscription.

www.plantphysiol.org/cgi/doi/10.1104/pp.108.131805

photosynthate: accumulation of soluble sugars has been reported in maize (*Zea mays*), wheat (*Triticum* spp.), tobacco (*Nicotiana tabacum*), tomato (*Solanum lycopersicum*), and Arabidopsis (*Arabidopsis thaliana*) infected with *Tobacco mosaic virus*, different *Pseudomonas* strains, smuts, rusts, and powdery mildews (Wright et al., 1995; Chou et al., 2000; Herbers et al., 2000; Scharte et al., 2005; Doehlemann et al., 2008). Consequently, the induction of sucrolytic cell wall invertase genes upon pathogen attack is now an established marker for source-to-sink transition in leaves (Herbers et al., 2000; Biemelt and Sonnewald, 2006; Swarbrick et al., 2006; Berger et al., 2007, and refs. therein). The reprogramming of the host metabolism and nutrient partitioning, in turn, triggers several signaling cascades. The modified carbohydrate metabolism represses photosynthetic genes and decreases photosynthetic activity, possibly by end-product inhibition (Nielsen et al., 1998; Roitsch, 1999; Smeekens, 2000; Truman et al., 2006; Kocal et al., 2008). The reduction of photosynthesis and assimilatory metabolic pathways allows the initiation of respiration and other processes required for defense. Interestingly, the high sugar levels that result from the induced sink metabolism also induce a number of defense-related genes (Herbers et al., 1996; Ehness et al., 1997; Herbers and Sonnewald, 1998; Berger et al., 2004; Scharte et al., 2005). Indeed, recent data suggest that cell wall invertases play an important role in host defense against pathogen attack (Essmann et al., 2008). Therefore, the hexose accumulation often observed has a dual role: on the one hand, it serves as nutrition for the microbe; on the other hand, it is part of the stress response of the plant aimed at eradicating the invading pathogen.

Upon infection with the Gram-positive, cytokinin-producing phytopathogen *Rhodococcus fascians*, the architecture of the plant is drastically changed (Crespi et al., 1992, 1994; Vereecke et al., 2000, 2002a, 2002b; Goethals et al., 2001; de O Manes et al., 2004). Remarkably little is known about the molecular basis of the pathologies of Gram-positive phytopathogens: they do not possess type III secretion systems, the typical Gram-negative effectors have not been identified, and no defense suppression mechanisms have been uncovered (Loria et al., 2006; Robert-Seilaniantz et al., 2007; Gartemann et al., 2008). Although it is becoming clear how *R. fascians* alters the shape of its hosts (Simón-Mateo et al., 2006; Depuydt et al., 2008, 2009), the establishment of an altered metabolic state had not been investigated until now. Therefore, with an integrated approach of genome-wide transcriptomics and primary metabolite profiling, we compared the response of Arabidopsis upon confrontation with two nearly isogenic *R. fascians* strains: the wild-type D188 that contains a linear virulence plasmid pFiD188, and its plasmid-free nonpathogenic derivative D188-5. Based on the obtained results, we propose a model for the role of the physiological alterations during initiation and maintenance of the interaction between Arabidopsis and *R. fascians*.

RESULTS

Transcriptome Analysis Underlines the Key Role for Cytokinins in Symptom Development

Arabidopsis plants that are infected with the phytopathogenic actinomycete *R. fascians* display typical phenotypes, such as smaller and serrated leaves, activated axillary and de novo formed meristems, and usually very compact rosettes (Vereecke et al., 2000; de O Manes et al., 2004; Simón-Mateo et al., 2006; Depuydt et al., 2008). To gain a genome-wide view of the processes that are involved in disease establishment, we compared the transcriptome of Arabidopsis plants (ecotype C24) infected with the virulent strain D188 with that of plants infected with the nonpathogenic derivative D188-5 as control samples using two-color CATMA microarrays (Crowe et al., 2003; Hilson et al., 2004). These arrays contain 24,576 gene-specific tags (GST) and probes for small open reading frames and 615 probes tiling the mitochondrial and chloroplastic genomes. For RNA preparation, plant material was harvested at three developmentally distinct time points: at 7 d postinfection (dpi) with the virulent *R. fascians* D188 strain, no clear symptoms were observed; at 14 dpi, the macroscopic phenotype became apparent; and at 24 dpi, Arabidopsis displayed the typical disease symptoms described above (Fig. 1A). Because the axillary regions are important for colonization, virulence gene expression, and symptom initiation by *R. fascians* (Cornelis et al., 2002), roots, cotyledons, and leaves were removed during harvesting. We selected a loop design as an experimental setup for the arrays (Fig. 1B) to evaluate gene expression as a function of time (see "Materials and Methods"). The choice of the control samples ensured the exclusion of genes that were merely triggered by the bacterial presence.

Statistical analysis indicated that 3,422 genes showed a significant treatment $\times$ time point interaction effect ($P < 0.001$; false discovery rate [FDR] < 0.0015; see "Materials and Methods"), of which 120 and 161 were more than 2-fold up- or down-regulated, respectively, in at least one time point (Fig. 1C; Tables I and II). The expression patterns obtained with the microarray hybridizations were confirmed for 10 genes randomly taken from the data set using quantitative reverse transcription (qRT)-PCR (Supplemental Fig. S1). The Gene Ontology (GO) annotation of the differentially expressed genes revealed that the major functional categories affected by *R. fascians* involved metabolism, response to (biotic/abiotic) stress, and transcription activity. Nevertheless, important modulations also occurred in the protein modification, transport, cell organization, and biogenesis categories (Fig. 2).

We examined the expression of all genes involved in cytokinin metabolism and the canonical cytokinin signaling pathway (Fig. 3). The expression of six A-type *ARABIDOPSIS RESPONSE REGULATOR* (*ARR*) genes, which are transcriptionally induced by cytokinins and

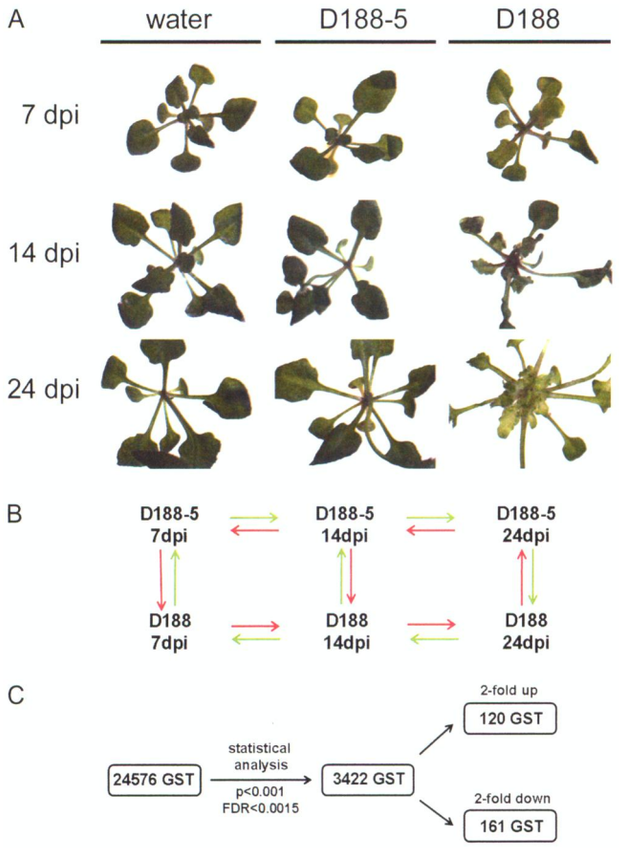

Figure 1. Sampling, setup, and analysis of microarray hybridizations of Arabidopsis plants infected with *R. fascians* D188-5 and D188. A, Phenotype at the selected time points. Roots, cotyledons, and leaves were removed for sampling. B, Experimental setup in a loop design for the 14 hybridizations. The dye swaps were combined with the two biological replicates. C, Flow chart representing the outcome of the statistical analysis of the microarray data.

mediate a feedback regulation of the cytokinin response (D'Agostino et al., 2000), and of the cytokinin receptor *AHK4* was activated, albeit at different levels. Moreover, two *CYTOKININ OXIDASE/DEHYDROGENASE* (*CKX*) genes were up-regulated and *ISOPENTENYL TRANSFERASE3* (*IPT3*) was down-regulated, illustrating the occurrence of cytokinin homeostasis and confirming previous data (Depuydt et al., 2008). *IPT8*, unlike *IPT3* not negatively regulated by cytokinins (Miyawaki et al., 2004), showed a minor up-regulation throughout infection. BiNGO analysis (Maere et al., 2005) of all up-regulated genes indicated a clear response toward a cytokinin stimulus, further underlining the central position of cytokinins in the *R. fascians* pathology (Supplemental Fig. S2).

The Genome-Wide Host Response toward *R. fascians* Infection Suggests a Highly Specialized Interaction

As the data presented above confirm the central role of cytokinins, we wondered how conserved the global transcriptional response upon *R. fascians* infection was when compared with cytokinin treatment and upon challenge with other pathogens. Therefore, biclustering analyses were done with the Genevestigator tool (Zimmermann et al., 2004) on the genes listed in Tables I and II in relevant publicly available data sets (zeatin treatment; infection with bacteria [*Agrobacterium tumefaciens* and *Pseudomonas syringae*], gray mold [*Botrytis cinerea*], two powdery mildews [*Erysiphe cichoracearum* and *Erysiphe orontii*], and an oomycete [*Phytophthora infestans*]). Generally, the transcriptional profiles of both the up- and down-regulated genes overlapped a little (Fig. 4). Approximately 12% of the down-regulated and 30% of the up-regulated transcripts were common between cytokinin treatment and *R. fascians* infection. Among the latter were cell wall-loosening expansins that have been implicated in cytokinin-induced cell proliferation (Downes and Crowell, 1998; Rashotte et al., 2003; indicated by u5, u11, and u14 in Fig. 4) and four *ARR* genes (indicated by u1, u8, u15, and u104 in Fig. 4). However, many of the transcriptional changes induced upon cytokinin treatment were not activated upon infection. For instance, *Bet v 1* genes, encoding putative cytokinin-detoxifying proteins, were induced by cytokinins (Mogensen et al., 2002; Brenner et al., 2005), but three family members were down-regulated upon *R. fascians* infection (Table II). Interestingly, the transcriptional overlap with *A. tumefaciens* was considerably higher, 38% and 45% of the down- and up-regulated genes, respectively, implying extensive similarities in the host response toward infection with both gall-forming bacteria. The more conserved up-regulation of a wound-responsive protein, a putative protease inhibitor, a putative chitinase, and two trypsin inhibitors (u20, u35, u41, u45, and u53 in Fig. 4) in many different treatments suggested that plant defense was activated during these biotic interactions. Intriguingly, in the *R. fascians* interaction, at 24 dpi most of these genes were down-regulated (Table I), hinting at an active down-regulation of defense.

R. fascians Actively Suppresses Defense

Detailed symptom analysis in tobacco and Arabidopsis did not point to a defense reaction of the plant in response to infection (de O Manes et al., 2001, 2004). As ROS are typically involved in restraining pathogen spread (Hammond-Kosack and Jones, 1996; Dempsey et al., 1999), we analyzed the microarray data set for genes related to ROS production or ROS scavenging. Five out of seven differential peroxidases (*PER21*, *PER33*, *PER50*, *PERATP23A*, and a putative peroxidase), together with a putative copper amino oxidase (At1g62810) that catalyzes the oxidative deamination of polyamines resulting in the release of hydrogen peroxide (H_2O_2), were significantly down-regulated upon infection with strain D188 (Table II; Supplemental Table S1), suggesting that *R. fascians* D188 colonization did not trigger H_2O_2 production. Indeed, no differential accumulation of H_2O_2 could be visualized

Table I. *Differentially up-regulated genes upon infection of Arabidopsis with R. fascians D188*

Gene	Function	Code[a]	Fold Change		
			7 dpi	*14 dpi*	*24 dpi*
Cell organization and biogenesis					
At1g26770	Expansin (putative; EXP10)	u14	1.45	3.39	4.76
At1g31580	Expressed protein	u101	2.89	0.86	0.95
At1g48920	Nucleolin (putative)	u82	0.95	1.32	2.13
At1g69530	Expansin (putative; EXP1)	u5	0.73	2.50	2.69
At2g03090	Expansin (putative; EXP15)	u92	0.81	1.69	4.22
At2g43590	Chitinase (putative)	u41	1.21	2.84	1.62
At2g43610	Glycoside hydrolase family 19 protein	u89	1.22	2.98	1.33
At3g18000	Phosphoethanolamine *N*-methyltransferase1 (PEAMT1)		0.58	1.40	2.27
At3g18080	Glycosyl hydrolase family 1 protein	u94	0.70	0.88	2.24
At4g08950	Phosphate-responsive protein (putative; EXO)	u54	1.49	0.62	2.29
At4g28250	β-Expansin (putative; EXPB3)	u11	0.60	1.86	4.30
Development					
At3g17520	Late embryogenesis abundant domain-containing protein	u102	0.99	0.94	2.76
At3g51810	Em-like protein GEA1 (EM1)	u99	1.03	1.05	3.61
At5g03840	Terminal flower 1 protein (TFL1)	u28	1.00	0.99	3.12
At5g57390	Ovule development protein (putative)	u36	1.23	1.46	2.01
At5g28640	SSXT protein-related/Gly-rich protein	u9	1.26	1.60	3.12
Electron transport or energy pathway					
At1g66540	Cytochrome P450 (putative)	u57	0.80	1.07	2.20
At4g27080	Thioredoxin family protein	u69	2.64	0.71	1.29
At5g49730	Ferric reductase-like transmembrane component family protein	u71	0.76	0.88	2.26
Metabolism					
At1g06080	Δ9 desaturase (ADS1)	u76	1.13	2.50	5.59
At1g30820	CTP synthase (putative)/UTP-ammonia ligase (putative)	u19	0.98	2.02	2.99
At1g56430	Nicotianamine synthase (putative)	u25	2.15	2.31	3.05
At1g80050	Adenine phosphoribosyltransferase 2 (APT2)	u77	1.57	2.06	4.44
At1g78580	Trehalose-6-phosphate synthase (putative)	u93	0.93	1.46	3.31
At3g21420	Oxidoreductase, 2OG-Fe(II) oxygenase family protein	u21	1.04	1.21	2.32
At3g30775	Pro oxidase, mitochondrial (POX; PRO1; ERD5)	u91	0.99	2.21	1.20
At3g57010	Strictosidine synthase family protein	u38	0.84	0.94	2.01
At3g63440	Cytokinin oxidase family protein	u105	0.99	1.48	2.26
At4g02290	Glycosyl hydrolase family 9 protein	u90	0.97	1.37	2.63
At4g30140	GDSL-motif lipase/hydrolase family protein	u87	1.45	2.93	2.06
At4g30290	Endoxyloglucan transferase (putative)	u40	1.65	2.48	5.88
At5g13930	Chalcone synthase/naringenin-chalcone synthase	u75	3.21	1.74	3.06
At5g17220	Glutathione *S*-transferase (putative)	u84	1.22	0.79	2.27
At5g18670	β-Amylase (putative; BMY3)	u81	0.56	1.11	2.16
At5g45670	GDSL-motif lipase/hydrolase family protein	u10	1.11	1.88	2.22
At5g51210	Gly-rich protein/oleosin	u50	1.12	0.97	2.39
At5g55250	*S*-adenosylmethionine:carboxyl methyltransferase family protein	u49	1.09	1.49	2.54
Protein metabolism					
At2g47020	Peptide chain release factor (putative)	u27	3.24	0.99	1.61
At4g25740	40S ribosomal protein S10 (RPS10A)	u51	1.30	1.25	2.01
At5g19110	Extracellular dermal glycoprotein (EDGP)-related	u16	1.45	2.21	1.23
At5g53450	Protein kinase family protein	u60	3.61	4.52	6.27
Response to biotic or abiotic stimulus					
At1g23130	Bet v I allergen family protein	u100	2.42	0.67	0.20
At1g56150	Auxin-responsive family protein	u26	2.22	1.52	0.61
At1g73260	Trypsin and protease inhibitor/Kunitz family protein	u45	2.05	1.12	0.65
At1g73330	Protease inhibitor (putative; DR4)	u61	2.06	0.65	0.13
At2g38310	Expressed protein	u52	2.31	1.00	1.04
At2g38870	Protease inhibitor (putative)	u35	2.62	1.61	0.50
At2g43510	Trypsin inhibitor (putative)	u53	2.12	1.46	0.67
At2g43530	Trypsin inhibitor (putative)	u56	2.20	0.60	0.45
At3g57240	β-1,3-Glucanase (BG3)	u29	1.07	2.17	1.73
At4g30660	Low-temperature and salt-responsive protein (putative)	u79	2.15	0.84	1.12
RNA/DNA metabolism					
At1g02840	Pre-mRNA splicing factor SF2 (SF2)/SR1 protein	u66	1.06	1.03	2.01
At3g27060	Ribonucleotide reductase (putative)	u42	1.45	2.08	2.21

(*Table continues on following page.*)

Table I. (*Continued from previous page.*)

Gene	Function	Code[a]	Fold Change		
Signal transduction					
At1g10470	Two-component-response regulator (ARR4)	u73	1.09	2.20	3.20
At1g19050	Two-component-response regulator (ARR7)	u1	1.81	3.75	8.88
At2g40670	Two-component-response regulator (ARR16)	u13	1.04	1.38	2.01
At2g41310	Two-component-response regulator (ARR8)	u8	1.01	1.37	2.24
At2g46070	Mitogen-activated protein kinase MAPK (putative; MPK12)	u86	0.96	1.00	2.31
At3g57040	Two-component-response regulator (ARR9)	u15	0.98	1.26	3.06
At5g15230	Gibberellin-regulated protein 4 (GASA4)/GA-responsive protein 4	u39	1.68	2.37	2.49
At5g62920	Two-component-response regulator (ARR6)	u104	1.65	2.80	6.57
Transcription factor					
At1g04250	Auxin-responsive protein/IAA-induced protein 17 (IAA17)	u55	1.37	1.58	2.26
At1g56170	Transcription factor (putative)	u78	1.51	1.07	2.01
At1g67260	Pseudogene (putative) cycloidea cyc4 protein		1.00	1.48	2.50
At1g68360	Zinc finger protein-related	u17	1.13	1.43	2.65
At1g71030	Myb family transcription factor	u23	0.56	0.73	2.35
At2g28510	Dof-type zinc finger domain-containing protein	u80	0.79	1.73	2.86
At3g15540	Auxin-responsive protein/IAA-induced protein 19 (IAA19)	u48	1.32	1.49	2.72
At3g16770	AP2 domain-containing protein RAP2.3 (RAP2.3)	u74	0.85	1.06	2.15
At3g25710	Basic helix-loop-helix (bHLH) family protein	u62	0.97	1.27	2.27
At4g37750	Ovule development protein aintegumenta (ANT)	u63	1.14	1.54	2.97
At5g25190	Ethylene-responsive element-binding protein (putative)	u58	1.28	2.15	4.11
At5g47370	Homeobox-Leu zipper protein 2 (HAT2)/HD-ZIP protein 2	u7	1.55	1.59	3.15
At5g50010	Expressed protein/similar to SAC51 transcription factor	u10	0.99	1.33	2.32
Transport					
At1g19450	Integral membrane protein (putative)/sugar transporter family protein	u103	0.99	1.49	2.09
At1g59740	Proton-dependent oligopeptide transport (POT) family protein	u24	1.29	1.51	3.09
At2g45180	Protease inhibitor/seed storage/lipid transfer protein (LTP)	u97	2.20	0.95	0.38
At3g25620	ABC transporter family protein		0.97	1.03	3.30
At3g25620	ABC transporter family protein	u46	0.86	0.88	5.88
At4g22520	Protease inhibitor/seed storage/lipid transfer protein (LTP)		3.10	4.91	3.10
At4g27780	Acyl-CoA binding protein 2 (ACBP2)	u109	1.03	1.11	2.02
At5g13740	Sugar transporter family protein	u83	1.51	1.67	2.41
At5g50200	Wound-responsive gene	u20	1.30	2.84	1.18
Others					
At1g02205	CER1 protein		1.08	1.06	2.33
At1g03870	Fasciclin-like arabinogalactan protein (FLA9)	u106	2.91	0.78	0.63
At1g48310	SNF2 domain-containing protein/helicase domain protein	u67	1.18	0.95	2.39
At1g66100	Thionin (putative)	u4	1.60	0.92	2.62
At1g70560	Alliinase C-terminal domain-containing protein	u33	1.17	1.90	2.60
At2g34700	Pollen Ole e 1 allergen and extensin family protein	u64	3.02	7.24	7.94
At3g09390	Metallothionein protein (putative; MT2A)	u22	2.24	0.79	1.01
At3g13520	Arabinogalactan protein (AGP12)	u31	2.47	0.82	0.89
At3g16640	Translationally controlled tumor family protein	u68	0.98	0.94	2.08
At4g04810	SelR domain-containing protein		2.40	0.62	0.38
At4g04830	SelR domain-containing protein	u111	2.94	0.65	0.30
At4g24780	Pectate lyase family protein	u85	0.71	1.24	2.10
At4g31290	ChaC-like family protein	u70	1.43	1.28	2.92
At5g48850	Male sterility MS5 family protein	u72	2.58	0.94	0.62
Unknown					
At1g15270	Expressed protein	u59	2.09	1.05	1.12
At1g29980	Expressed protein	u34	1.15	1.65	2.16
At1g64980	Expressed protein	u88	1.39	2.27	2.42
At1g68250	Expressed protein	u43	0.90	0.87	2.71
At2g27385	Expressed protein		1.24	1.11	2.12
At2g30760	Hypothetical protein	u44	1.28	1.50	3.03
At2g32280	Expressed protein	u18	1.27	1.56	2.03
At2g32560	F-box family protein		1.18	1.26	2.49
At2g34160	Expressed protein	u47	2.06	1.19	1.04
At2g39870	Expressed protein	u12	0.96	1.11	2.32
At3g05730	Expressed protein	u96	1.26	2.25	1.89
At3g08030	Expressed protein	u30	0.93	1.36	2.73

(*Table continues on following page.*)

Table I. *(Continued from previous page.)*

Gene	Function	Code[a]	Fold Change		
At3g11720	Expressed protein		1.00	1.39	2.14
At3g16660	Expressed protein	u110	1.10	2.63	1.67
At3g19200	Hypothetical protein	u107	1.10	1.54	3.59
At3g56360	Expressed protein	u65	1.07	1.25	2.85
At4g09840	Expressed protein	u95	1.07	0.97	2.07
At4g30410	Expressed protein	u2	1.20	1.58	2.94
At5g03545	Expressed protein	u37	3.21	1.07	0.25
At5g05250	Expressed protein	u32	1.32	1.72	2.78
At5g19260	Expressed protein	u3	1.21	1.76	3.98
At5g24660	Expressed protein	u98	3.40	1.14	0.63
At5g52900	Expressed protein	u6	1.17	1.64	3.22

[a]Refers to genes in the left panel of Figure 4.

by 3,3′-diaminobenzidine (DAB) staining of infected Arabidopsis plants at different time points during the interaction (data not shown), and the oxidative stress marker thioredoxin H5 (*TRX-h5*; Laloi et al., 2004) was severely repressed (Table II). Moreover, the expression of (stromal) L-ascorbate peroxidase (*APX1* and *sAPX*), glutathione peroxidase (*GPX5* and *GPX6*), copper-zinc superoxide dismutase (*CSD1* and *CSD2*), and catalase (*CAT1* and *CAT2*) genes, known to be ROS scavengers (Mittler et al., 2004), was also down-regulated upon infection with strain D188 (Table II; Supplemental Table S1). Furthermore, dehydroascorbate reductase (*DHAR3*) and monodehydroascorbate reductase 4 (*MDAR4*) and *MDAR5*, which convert dehydroascorbate to the antioxidant ascorbate, were repressed (Table II; Supplemental Table S1). The latter transcript data were supported by the strong reduction in ascorbate levels and the accumulation of its precursor dehydroascorbate in infected tissues (Supplemental Fig. S3). Finally, the genes encoding ferritin 2 and 3, hypothesized to protect cells against ROS by regulating the amount of Fe(II) and Fe(III) (Murgia et al., 2001), were also severely repressed (Table II). Altogether, these data indicated that infection with *R. fascians* does not cause an oxidative burst in the plant.

Next, we analyzed the microarray data set for genes encoding (putative) pathogenesis-related proteins, such as (endo)glucanases, chitinases, proteinase inhibitor proteins, thionins, glutathione *S*-transferases, lipid transfer proteins, Phe ammonia lyases, and chalcone synthases known to function in defense (Jwa et al., 2006). Although a few genes were up-regulated throughout *R. fascians* infection, most were down-regulated in the later stages (Supplemental Table S1), among them established defense markers, such as Phe ammonia lyases, suggesting active defense suppression by *R. fascians* D188.

To get a clue on which bacterial signal could be involved in defense suppression, we evaluated the expression of the differentially expressed stress-related genes upon D188 infection (Fig. 5A for Table II, Fig. 5B for Supplemental Table S1) in data sets obtained from other biotic interactions and cytokinin and auxin treatments. Interestingly, except for *A. tumefaciens*, expression of most genes was up-regulated in the selected biotic interactions (Fig. 5A). Unexpectedly, zeatin treatment activated the expression of almost all analyzed genes (Fig. 5), while auxin had either no effect or a repressing effect, implying that auxin secretion by *R. fascians* might be involved in defense avoidance.

R. fascians Reprograms the Host Primary Metabolism

GO annotation revealed that genes involved in metabolism constituted 11% and 12% of the down- and up-regulated genes, respectively. Moreover, BiNGO analysis of the down-regulated genes implied an impact on tricarboxylic acid (TCA) cycle intermediate metabolism and on (branched chain) amino acid and derivative catabolism (Supplemental Fig. S3). These transcript data suggested that infection might significantly modulate the primary metabolism of the plant. For a more comprehensive view, profiles of 38 primary metabolites were analyzed by gas chromatography-mass spectrometry (GC-MS) of extracts prepared from complete Arabidopsis shoots at 4, 7, 14, and 24 dpi treated as follows: mock inoculation with water, control infection with strain D188-5, or infection with strain D188. Although this study is focused on the differences between D188-5 and D188 infections, to correlate metabolic shifts with disease development, we noticed that for some metabolites D188-5 infection caused notable changes compared with mock-inoculated controls (indicated by # in Figs. 6, 10, and 11 and Supplemental Fig. S4), which could be correlated with a general reaction to bacterial colonization or with early flowering, which is a conserved developmental response on bacterial infection (Korves and Bergelson, 2003). Generally, almost 66% of the tested metabolites exhibited similar profiles over time for the three treatments, although in 50% of these cases the final concentration differed significantly from that of the controls. For the remaining 34% of the metabolites, the profiles were completely dissimilar (Figs. 6, 10, and 11; Supplemental Fig. S4).

Table II. *Differentially down-regulated genes upon infection of Arabidopsis with R. fascians D188*

Gene	Function	Code[a]	Fold Change		
			7 dpi	*14 dpi*	*24 dpi*
Biotic/abiotic stress					
At1g23130	Bet v I allergen family protein	d131	2.42	0.67	0.20
At1g54040	Kelch repeat-containing protein	d129	0.98	0.63	0.46
At1g70850	Bet v I allergen family protein	d94	0.96	0.59	0.25
At1g70880	Bet v I allergen family protein	d61	1.09	0.73	0.48
At2g15490	UDP-glucoronosyl/UDP-glucosyl transferase family protein	d31	1.27	0.98	0.48
At2g18420	Gibberellin-responsive protein (putative)	d73	1.10	0.79	0.27
At2g35980	HIN1 family protein	d85	1.39	1.00	0.45
At2g45210	Auxin-responsive protein-related	d109	0.97	0.74	0.42
At3g28930	avrRpt2-induced AIG2 protein (AIG2)	d70	1.13	0.90	0.47
At5g14920	Gibberellin-regulated family protein	d133	1.45	0.99	0.49
At5g53160	Expressed protein	d110	0.87	1.02	0.42
Cell organization and biogenesis					
At4g36380	Cytochrome P450 90C1 (CYP90C1)/rotundifolia3 (ROT3)	d107	0.92	0.81	0.44
At5g66540	Expressed protein	d36	1.31	0.72	0.41
Development					
At1g02820	Late embryogenesis abundant 3 (LEA3) family protein	d145	1.74	0.76	0.26
At4g02380	Late embryogenesis abundant 3 (LEA3) family protein	d140	1.72	0.78	0.26
DNA and RNA metabolism					
At5g64200	Arg/Ser-rich splicing factor SC35	d91	1.41	0.64	0.45
Electron transport or energy pathway					
At1g26410	FAD-binding domain-containing protein	d144	1.48	0.98	0.40
At2g44790	Uclacyanin II	d86	0.84	0.91	0.35
At3g22370	Alternative oxidase 1a, mitochondrial (AOX1A)	d84	1.13	0.90	0.43
At3g56060	Glc-methanol-choline (GMC) oxidoreductase family protein	d87	0.81	0.67	0.32
At4g15760	Monooxygenase (putative; MO1)		1.03	0.82	0.50
At4g15765	Monooxygenase family protein		0.85	0.75	0.40
At4g38540	Monooxygenase (putative; MO2)	d46	1.16	0.87	0.47
At5g36220	Cytochrome P450 81D1 (CYP81D1; CYP91A1)	d138	1.12	0.97	0.48
Metabolism					
At1g05010	Ethylene-forming enzyme (ACO; EAT1)	d111	1.02	1.15	0.48
At1g21440	Mutase family protein	d5	0.44	0.50	0.77
At1g24100	UDP-glucoronosyl/UDP-glucosyl transferase family protein	d34	0.45	0.69	0.83
At1g64660	Cys/Met metabolism pyridoxal-phosphate-dependent enzyme	d113	1.30	0.83	0.28
At2g25450	2-Oxoglutarate-dependent dioxygenase (putative)	d55	0.54	0.44	0.22
At2g26560	Patatin (putative)	d108	1.40	0.66	0.41
At3g08860	β-Ala-pyruvate aminotransferase (putative)/AGT (putative)	d142	1.01	0.69	0.43
At3g09260	Glycosyl hydrolase family 1 protein	d96	1.14	1.16	0.48
At3g09270	Glutathione *S*-transferase (putative)	d77	1.02	0.96	0.50
At3g13450	Branched chain α-keto acid dehydrogenase E1 β-subunit (DIN4)	d143	1.01	0.83	0.47
At3g14990	4-Methyl-5(β-hydroxyethyl)-thiazole-monophosphate bios (putative)	d75	0.96	0.83	0.44
At3g19710	Branched chain amino acid aminotransferase (putative; BCAT4)	d16	0.46	0.57	1.25
At3g29250	Short-chain dehydrogenase/reductase (SDR) family protein	d83	1.06	0.89	0.46
At3g44300	Nitrilase 2 (NIT2)	d150	1.43	0.72	0.10
At3g48990	AMP-dependent synthetase and ligase family protein	d25	0.93	0.73	0.47
At3g58990	Aconitase C-terminal domain-containing protein	d20	0.40	0.53	1.45
At3g60130	Glycosyl hydrolase family 1/β-glucosidase (putative; YLS1)	d28	1.02	0.87	0.36
At4g13250	Short-chain dehydrogenase/reductase (SDR) family protein	d54	0.37	0.48	0.31
At4g13430	Aconitase family protein/aconitate hydratase family protein	d130	0.40	0.49	0.72
At4g15530	Pyruvate phosphate dikinase family protein	d63	0.87	0.78	0.47
At4g28780	GDSL-motif lipase/hydrolase family protein	d103	1.04	0.71	0.30
At5g07440	Glu dehydrogenase 2 (GDH2)	d148	1.13	0.95	0.38
At5g02780	In2-1 protein (putative)	d73	1.89	0.91	0.31
At5g09440	Phosphate-responsive protein (putative)	d56	1.32	0.50	0.32
At5g09530	Hyp-rich glycoprotein family protein	d22	1.25	0.88	0.46
At5g17380	Pyruvate decarboxylase family protein	d53	0.78	0.91	0.49
At5g23020	2-Isopropylmalate synthase 2 (IMS2)	d11	0.64	0.66	0.34
At5g23660	Nodulin MtN3 family protein	d68	1.86	0.63	0.47
At5g44020	Acid phosphatase class B family protein	d122	1.50	0.81	0.27
At5g44930	Exostosin family protein	d127	1.06	0.64	0.36

(*Table continues on following page.*)

Table II. (*Continued from previous page.*)

Gene	Function	Code[a]	Fold Change		
At5g49360	Glycosyl hydrolase family 3 protein	d152	1.04	0.53	0.38
At5g51970	Sorbitol dehydrogenase (putative)/L-iditol 2-dehydrogenase (putative)	d39	0.98	0.70	0.48
At5g59530	2-Oxoglutarate-dependent dioxygenase (putative)	d37	1.23	0.99	0.47
At5g65010	Asn synthetase 2 (ASN2)	d88	1.03	0.91	0.44
Protein modification					
At1g72070	DNAJ heat shock N-terminal domain-containing protein	d80	1.86	0.65	0.32
At3g01290	Band 7 family protein	d134	1.18	0.91	0.45
At4g16563	Aspartyl protease family protein	d93	1.31	0.67	0.48
At4g38690	1-Phosphatidylinositol phosphodiesterase-related	d2	1.06	0.64	0.50
At5g23210	Ser carboxypeptidase S10 family protein	d146	1.26	0.71	0.48
AtCg00670	ATP-dependent Clp protease proteolytic subunit		1.05	0.86	0.47
Response to stress					
At1g07890	L-Ascorbate peroxidase 1, cytosolic (APX1)	d42	0.59	0.66	0.40
At1g08830	Copper/zinc superoxide dismutase (CSD1)	d92	0.38	1.43	0.86
At1g09560	Germin-like protein (GLP4; GLP5)	d44	1.23	0.78	0.36
At1g45145	Thioredoxin H-type 5 (TRX-h5; TOUL)	d102	1.37	0.69	0.41
At1g73330	Protease inhibitor (putative; DR4)	d69	2.06	0.65	0.13
At2g23680	Stress-responsive protein (putative)	d71	1.36	0.76	0.37
At2g28190	Copper/zinc superoxide dismutase (CSD2)	d106	0.44	1.18	1.12
At2g37130	Peroxidase 21 (PER21; P21; PRXR5)	d8	0.74	0.52	0.31
At2g37180	Water stress-induced tonoplast intrinsic protein (RD28)	d49	0.84	0.84	0.46
At2g38870	Protease inhibitor (putative)	d45	2.62	1.61	0.50
At2g39800	Δ1-Pyrroline-5-carboxylate synthetase A/P5CS A (P5CS1)	d95	0.48	0.70	1.94
At3g50970	Dehydrin xero2 (XERO2)/low-temperature-induced protein LTI30	d67	1.27	0.47	0.45
At4g02520	Glutathione *S*-transferase (putative)	d119	1.10	0.73	0.21
At4g08390	L-Ascorbate peroxidase, stromal (sAPX)	d149	0.43	0.68	0.38
At4g25100	Superoxide dismutase (Fe), chloroplast (SODB; FSD1)	d120	0.67	0.41	0.24
At4g35770	Senescence-associated protein (SEN1)	d38	1.37	0.81	0.42
At4g37530	Peroxidase 50 (PER50; PRXR50)	d132	0.68	0.75	0.42
At5g14780	Formate dehydrogenase (FDH)	d79	0.74	0.80	0.45
Signal transduction					
At1g02340	Reduced phytochrome signaling (REP1; BHLH26)	d29	0.86	0.55	0.27
At4g30270	MERI-5 protein (MERI-5; MERI5B)	d116	1.66	0.48	0.28
At5g15410	Cyclic nucleotide-gated channel (CNGC2)	d3	0.97	0.84	0.48
Transcription factor					
At2g36890	Myb family transcription factor (MYB38)	d51	0.99	0.90	0.48
At2g43060	Expressed protein	d59	1.17	0.72	0.39
At2g46970	Basic helix-loop-helix (bHLH) protein (putative)		1.18	0.68	0.23
At3g05690	CCAAT-binding transcription factor (CBF-B/NF-YA) family protein	d32	0.87	0.69	0.43
At3g51910	Heat shock transcription factor family protein	d24	1.13	0.87	0.45
At3g56400	WRKY family transcription factor	d105	0.46	1.20	1.62
At3g60530	Zinc finger (GATA type) family protein	d26	1.35	0.93	0.37
At5g07690	Myb family transcription factor (MYB29)	d7	0.33	0.53	1.05
At5g07700	Myb family transcription factor (MYB76)	d125	0.35	0.51	1.28
At5g23000	Myb family transcription factor (MYB37)	d114	1.04	0.81	0.49
At5g53980	Homeobox-Leu zipper family protein	d136	0.87	1.07	0.49
At5g63790	No apical meristem (NAM) family protein	d43	0.62	0.97	0.41
Transport					
At1g08230	Amino acid transporter family protein	d115	1.02	0.79	0.46
At1g66760	MATE efflux family protein	d101	1.16	0.85	0.47
At1g78000	Sulfate transporter (Sultr1;2)	d76	1.54	0.57	0.47
At1g80830	NRAMP metal ion transporter 1 (NRAMP1)	d82	0.68	0.67	0.37
At2g10940	Protease inhibitor/seed storage/lipid transfer protein (LTP)	d153	0.85	0.91	0.37
At2g26650	Potassium channel protein 1 (AKT1)	d104	1.15	0.74	0.44
At2g40300	Ferritin (putative)	d123	0.78	0.79	0.42
At2g45180	Protease inhibitor/seed storage/lipid transfer protein (LTP)	d17	2.20	0.95	0.38
At3g48970	Copper-binding family protein	d97	1.15	0.85	0.48
At3g53980	Protease inhibitor/seed storage/lipid transfer protein (LTP)	d30	1.68	0.48	1.18
At3g56090	Ferritin (putative)	d14	1.03	1.07	0.48
At3g56200	Amino acid transporter family protein	d52	1.90	0.69	0.44
At4g00370	Sugar transporter family protein	d12	1.22	0.77	0.43

(*Table continues on following page.*)

Table II. (*Continued from previous page.*)

Gene	Function	Code[a]	Fold Change		
At4g04770	ATP-binding cassette transporter (ABC1)	d9	0.36	0.46	0.40
At4g12030	Bile acid:sodium symporter family protein	d1	0.38	0.48	1.26
At4g30110	ATPase E1-E2-type family protein	d6	0.77	0.54	0.41
At5g10180	Sulfate transporter	d10	0.46	0.42	0.14
At5g61520	Hexose transporter (putative)	d60	1.23	0.81	0.45
At5g62670	ATPase, plasma membrane-type (putative)/proton pump (putative)	d128	0.82	0.84	0.46
Others					
At1g02850	Glycosyl hydrolase family 1 protein	d126	1.11	1.01	0.43
At1g04660	Gly-rich protein	d117	0.99	0.61	0.47
At1g18590	Sulfotransferase family protein	d4	0.40	0.56	1.66
At1g49320	BURP domain-containing protein	d78	0.57	0.48	0.33
At1g76590	Zinc-binding family protein	d58	1.00	0.65	0.36
At1g76800	Nodulin (putative)	d13	0.88	0.63	0.30
At1g78830	Curculin-like (Man-binding) lectin family protein	d48	1.24	0.72	0.34
At2g03890	Phosphatidylinositol 3- and 4-kinase family protein	d139	1.22	0.96	0.45
At2g05440	Gly-rich protein	d135	1.39	0.54	0.09
At2g05540	Gly-rich protein	d74	0.84	0.78	0.39
At2g32870	MATH domain-containing protein	d141	0.77	0.48	0.62
At2g39030	GCN5-related *N*-acetyltransferase (GNAT) family protein	d50	1.32	0.81	0.37
At2g39310	Jacalin lectin family protein	d100	1.05	0.80	0.48
At2g39330	Jacalin lectin family protein	d35	0.78	0.46	0.41
At2g41380	Embryo-abundant protein-related	d147	1.33	0.90	0.47
At2g43530	Trypsin inhibitor (putative)	d65	2.20	0.60	0.45
At3g04720	Hevein-like protein (HEL)	d90	1.50	0.73	0.13
At3g15356	Legume lectin family protein		1.16	0.71	0.21
At3g22740	Homocysteine *S*-methyltransferase 3 (HMT-3)	d18	0.34	0.60	1.09
At3g48390	MA3 domain-containing protein		1.01	0.77	0.47
At3g50440	Hydrolase, α/β-fold family protein	d15	1.00	0.61	0.35
At3g50440	Hydrolase, α/β-fold family protein		0.99	0.70	0.45
At3g54600	DJ-1 family protein		0.46	0.58	1.02
At4g00780	MATH domain-containing protein	d64	0.84	0.49	0.97
At4g01440	Nodulin MtN21 family protein	d121	0.93	0.83	0.50
At4g04810	SelR domain-containing protein		2.40	0.62	0.38
At4g04830	SelR domain-containing protein	d21	2.94	0.65	0.30
At4g15610	Integral membrane family protein	d137	1.48	0.74	0.24
At4g28050	Senescence-associated protein (putative)	d99	1.10	0.57	0.25
At4g36850	PQ-loop repeat family protein/transmembrane family protein		0.99	0.65	0.46
At4g38080	Hyp-rich glycoprotein family protein	d98	1.58	0.80	0.33
At4g39940	Adenylylsulfate kinase 2 (AKN2)	d112	0.39	0.59	1.13
Unknown					
At1g01430	Expressed protein	d72	0.96	0.78	0.49
At1g07090	Expressed protein	d40	1.26	0.85	0.46
At1g10090	Expressed protein	d27	0.92	0.60	0.37
At1g29050	Expressed protein	d41	1.18	0.66	0.45
At1g49310	Expressed protein	d89	0.85	0.66	0.45
At1g54740	Expressed protein	d62	0.78	0.66	0.48
At1g73810	Expressed protein		1.05	0.65	0.44
At2g04795	Expressed protein	d19	1.24	0.63	0.42
At3g19030	Expressed protein	d124	1.61	0.71	0.49
At3g28320	Hypothetical protein	d66	0.78	0.83	0.34
At4g31330	Expressed protein	d118	1.01	0.70	0.49
At4g32480	Expressed protein		0.93	0.62	0.36
At5g01740	Expressed protein	d23	1.43	0.75	0.28
At5g03545	Expressed protein	d47	3.21	1.07	0.25
At5g40450	Expressed protein		0.87	0.88	0.49
At5g40450	Expressed protein	d151	1.46	0.86	0.47
At5g45410	Expressed protein	d81	0.62	0.74	0.47
At5g64090	Expressed protein	d57	1.49	0.49	0.52

[a]Refers to genes in the right panel of Figure 4.

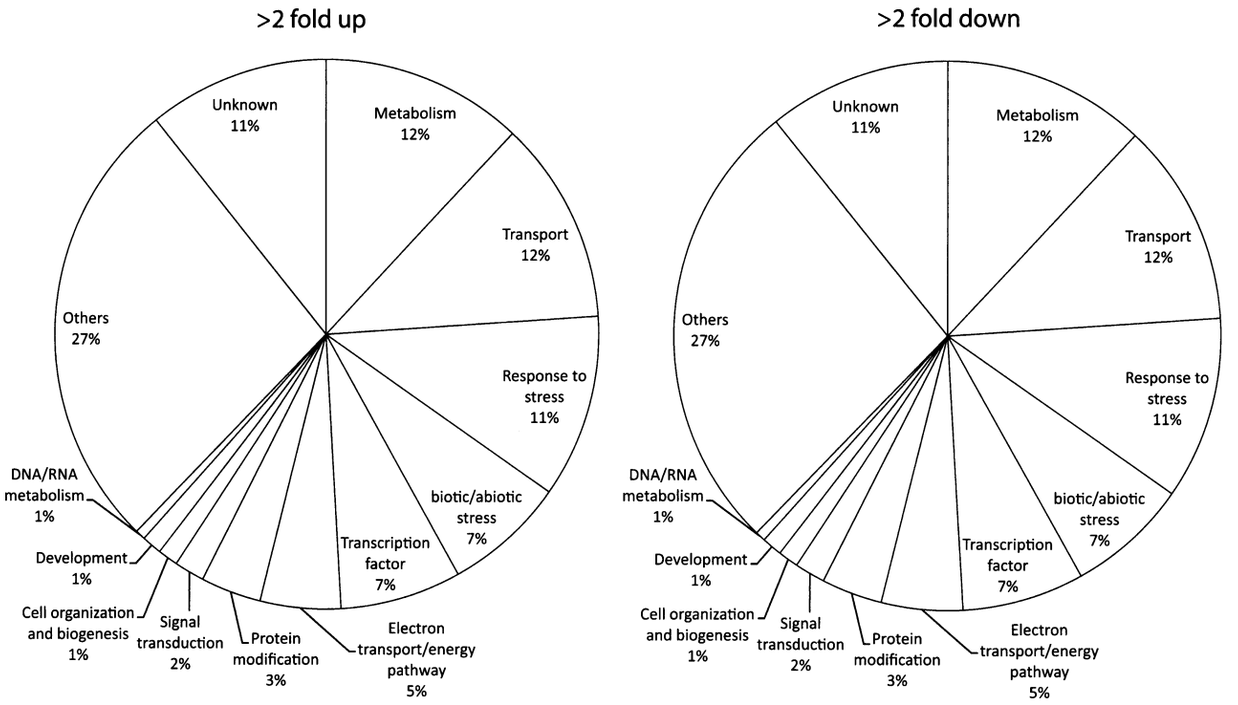

Figure 2. GO annotation of the 2-fold differentially up- and down-regulated genes upon *R. fascians* infection.

R. fascians Infection Triggers Sink Development in Symptomatic Tissues

During plant development, but also upon pathogen infections, source-to-sink transitions occur in tissues, with the conversion from a sugar-producing and -exporting status to a sugar-importing and -accumulating status as a result. Interestingly, throughout the experiment, the total sugar content of shoots was between 2.5- and 2.9-fold higher upon D188 infection than that of the mock-infected control. While Suc levels did not differ from 4 dpi onward, the concentrations of the hexoses Glc, Fru, and sorbose as well as of the disaccharide maltose and of the trisaccharide raffinose increased strongly (Fig. 6). For the sugar alcohols, galactinol accumulated in both D188- and D188-5-infected tissues, albeit with different kinetics, whereas erythritol levels only increased upon D188-5 infection. The profiles for glycerol and glycerol-3-phosphate were comparable for the three treatments, whereas the concentration of myoinositol was somewhat higher upon infection. The most striking difference was observed for the nonreducing disaccharide trehalose, which accumulated upon infection with strain D188-5 and strain D188 at 4 dpi between 64- and 42-fold, respectively. At 24 dpi, the level of trehalose strongly decreased in D188-5-infected tissue and was 5-fold higher in the D188-infected plants. The microarray data indeed showed that a trehalose phosphate synthetase gene, *TPS1*, encoding the first step of trehalose biosynthesis, was differentially up-regulated from 14 dpi onward (Table I). No differential expression was measured for trehalose-6-phosphate-phosphatase genes that mediate the final dephosphorylation step to trehalose.

The specific increase in the hexose-Suc ratio only upon *R. fascians* D188 infection hinted at a possible involvement of invertases. In the microarray data set, no differentially expressed invertase genes were present; however, it could not be ruled out that this was caused by the different sampling for metabolome and transcriptome analysis. Therefore, we examined the

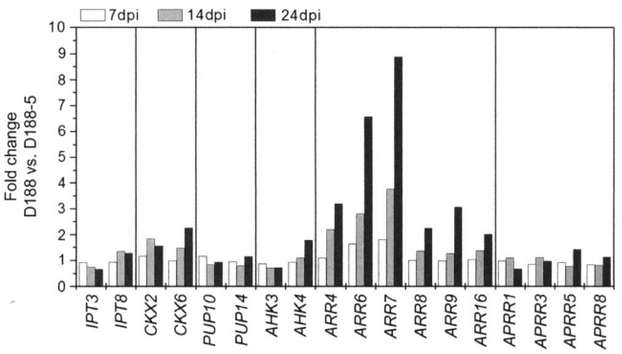

Figure 3. Differentially expressed cytokinin-associated genes during the *R. fascians* plant interaction at 7, 14, and 24 dpi detected via microarray hybridizations. Fold changes between *R. fascians* D188 and D188-5 (control) are presented.

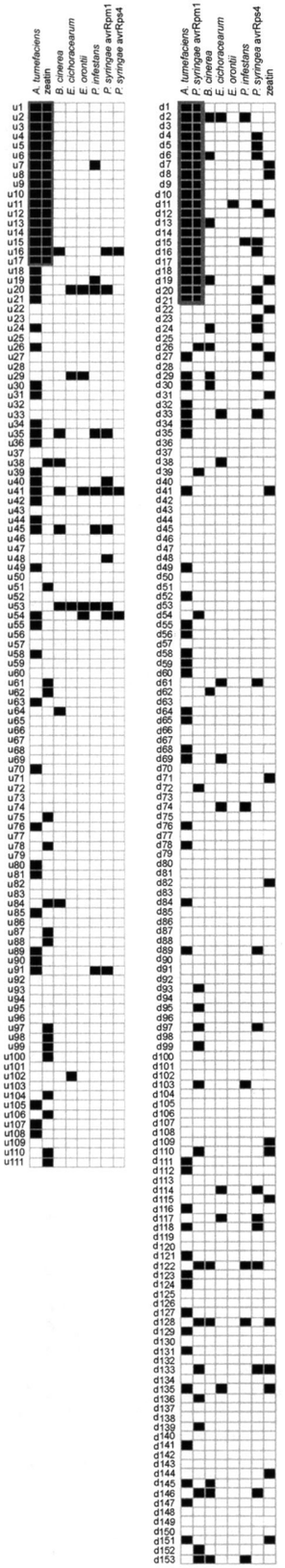

expression pattern of cell wall (*FRUCT1*), cytoplasmic (*FRUCT3* and *FRUCT4*), and vacuolar and chloroplastic invertase (*INV-H* and *INV-E*, respectively) genes in complete shoot tissues at 4, 7, 14, and 24 d after treatment by RT-PCR (Fig. 7A). The expression of the cell wall invertase gene was already induced at 4 dpi by both bacterial infections (D188-5 and D188), but the induction was stronger and only persisted throughout the experiment upon infection with strain D188. A comparable, although less marked, pattern was obtained for *FRUCT3*, while *FRUCT4* was not differentially expressed. For *INV-H*, no clear pattern was observed, although at 24 dpi the expression was highest in D188-infected plants. Finally, the *INV-E* expression profile resembled that of *FRUCT1*. These transcript profiles and the hexose metabolite data were confirmed by measuring invertase enzyme activities in infected and control shoot material. Indeed, for all three invertase types, the enzyme activities were significantly higher upon D188 infection. In agreement with the RT-PCR data, a differential activity could also be measured for the cell wall-bound invertase in D188-5-infected tissue (Fig. 7B).

Photosynthesis upon D188 Infection: Reduced Activity and Enhanced Competition

Hexoses presumably down-regulate photosynthetic activity and photosynthesis gene expression and thus influence the source/sink status of the plant tissues (Biemelt and Sonnewald, 2006). Given the accumulation of hexoses and the typical sink-associated invertase activity in D188-infected plants, we investigated the effect of infection on photosynthesis. The pale green color of symptomatic Arabidopsis plants (Fig. 1A) already hinted at an altered photosynthetic capacity. The loss of chlorophyll during symptom establishment was indeed confirmed by spectrophotometric analysis (Fig. 8A). Among the down-regulated genes identified in the microarray (Table II), 5% was classified in the GO category "Electron transport/energy pathway" (Fig. 2). Interestingly, At2g28000 and At1g55490, encoding the α- and β-subunits of chaperonin-60, a molecular chaperone involved in correct Rubisco folding and, thus, activity (Salvucci, 2008), were found to be significantly down-regulated in our data set, although by less than 2-fold (data not shown). Since leaves were not harvested for the microarray experiment, the expression of the photosynthesis marker genes *RbcS* and *CAB2* was investigated with RT-PCR on RNA extracted

Figure 4. Output of Genevestigator bicluster analyses comparing *R. fascians* infection with hormone treatment and biotic interactions. Rows represent the up-regulated (left) and down-regulated (right) genes, and the coded identities of the genes are given in Tables I and II, respectively. Black squares mark matching expression profiles for *R. fascians*-infected samples and the considered treatment (www.genevestigator.ethz.ch). [See online article for color version of this figure.]

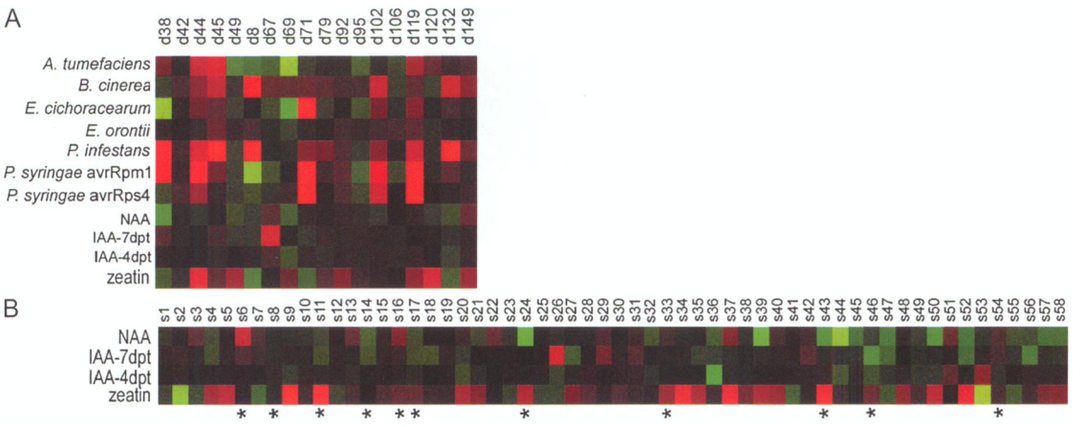

Figure 5. Genevestigator study of the stress- and defense-related genes upon *R. fascians* infection. A, Down-regulated stress-related genes of Table II and their response upon different biotic interactions and hormone treatments. B, Responses of all differentially regulated defense-related genes after *R. fascians* infection (Supplemental Table S1) and their responses upon hormone treatment. Genes that are down-regulated in at least one time point upon *R. fascians* infection are not marked, while asterisks indicate up-regulated genes throughout *R. fascians* infection. Green and red represent genes that are down- and up-regulated, respectively. Black indicates no significant changes. IAA, Indole-3-acetic acid; NAA, naphthaleneacetic acid.

from complete shoots. Generally, D188-5 infection had no or little effect on the age-dependent decline of *RbcS* and *CAB2* expression levels. In contrast, upon D188 infection, both *RbcS* and *CAB2* were significantly down-regulated already at 4 dpi (Fig. 8B). The photosynthetic capacity of infected plants was further assessed by chlorophyll fluorescence imaging (Fig. 8, C–F). Chlorophyll fluorescence is indicative of the overall rate of the photosynthetic function and can be used to determine the efficiency of PSII photochemistry under biotic and abiotic stress conditions (Maxwell and Johnson, 2000; Quilliam et al., 2006). The effective quan-

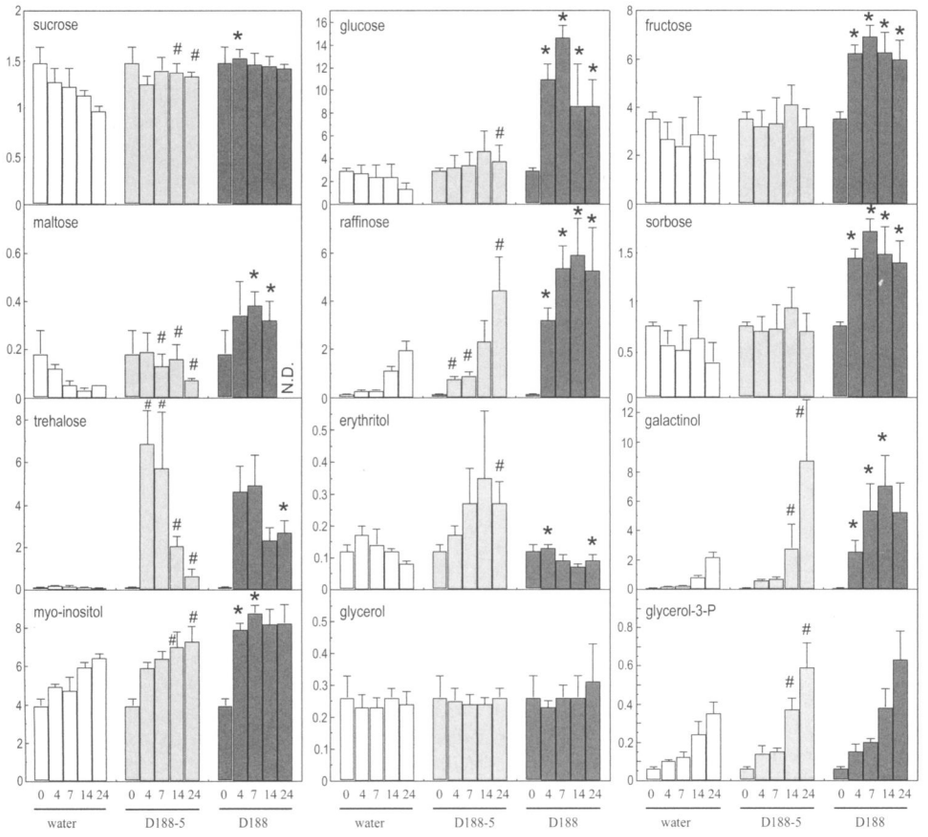

Figure 6. Effect of *R. fascians* infection on carbon metabolism in planta. Inoculation with water, *R. fascians* D188-5, and D188 at 4, 7, 14, and 24 dpi. Symbols (# and *) indicate statistically significant differences between D188-5 and mock-infected samples ($P < 0.01$) and between D188-5 and D188 samples ($P < 0.01$), respectively. The metabolite abundances are expressed relative to the internal standard ribitol at each time point and normalized to the fresh weight. Error bars represent SD ($n = 6$). N.D., Not determined.

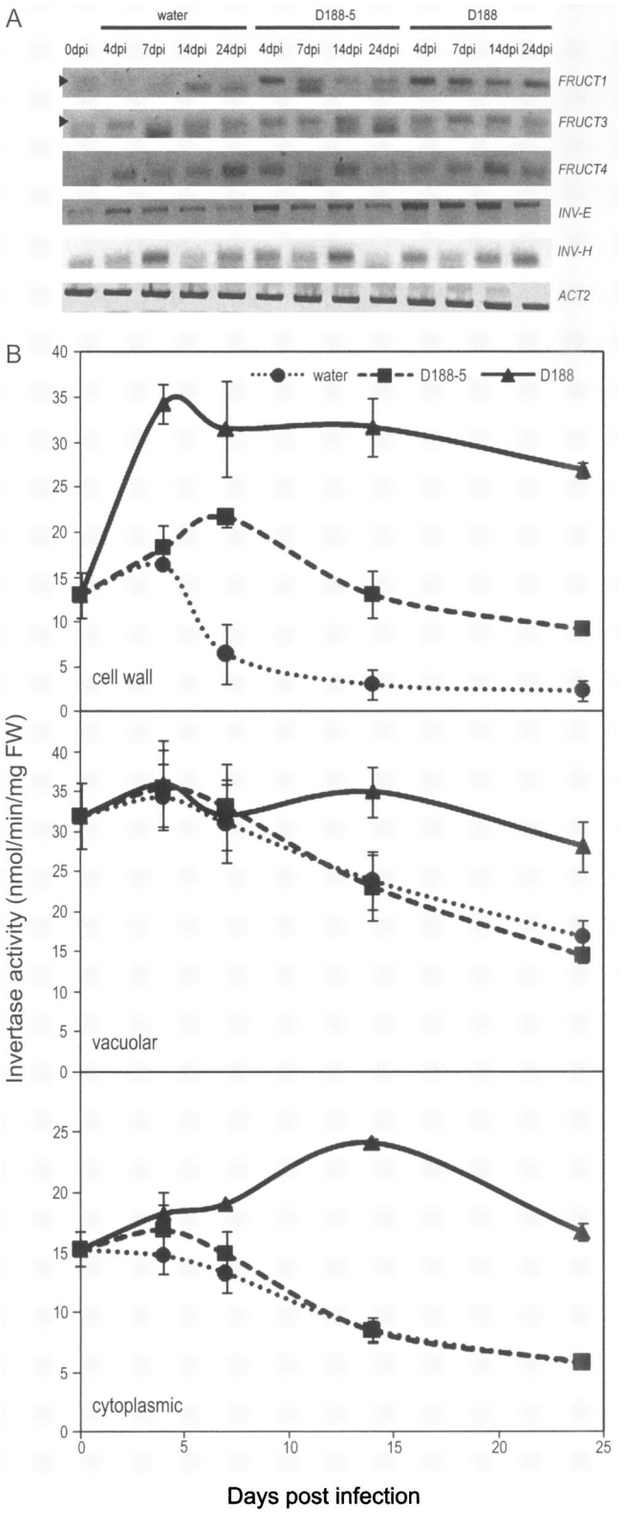

Figure 7. Invertase gene expression and activities upon *R. fascians* infection. RT-PCR profiling of five invertase genes (A) and enzymatic activities of the cell wall, vacuolar, and cytoplasmic invertases (B) after inoculation with water, *R. fascians* D188-5, and D188. FW, Fresh weight.

tum yield of PSII [Y(II)], the maximum quantum yield of PSII (F_v/F_m), and the nonphotochemical quenching parameters NPQ and qN (see "Materials and Methods") were measured during *R. fascians* infection. Figure 8C shows a false-color-coded image of Y(II) that represents the proportion of absorbed light that will be used for electron transport through PSII. Whereas Y(II) was not significantly altered by infection of Arabidopsis with strain D188-5, it was markedly reduced by D188 infection. The decrease in Y(II) started at 7 dpi at the leaf edges and, with time, spread throughout the whole leaf. Interestingly, *R. fascians* colonization starts with the formation of microcolonies at leaf edges (Fig. 9A; Cornelis et al., 2001), suggesting that local secretion of morphogens by the bacteria directly affects photosynthesis. Infected *ARR5:GUS* lines indeed showed a patchy expression pattern in leaves, which is mostly confined to the margins (Fig. 9B). *CKX* genes are instrumental for cytokinin degradation and homeostasis upon infection of Arabidopsis with *R. fascians* (Depuydt et al., 2008; Pertry et al., 2009). Spot inoculation on leaves of *CKX5:GUS* and *CKX6:GUS* marker lines revealed a colocalization of the cytokinin-secreting *R. fascians* colonies and GUS staining (Fig. 9C), further supporting the localized action of the bacterial signals.

The F_v/F_m, a measure of the intrinsic efficiency of PSII, was also significantly lower upon D188 infection (Fig. 8D), indicating photoinhibition. The qN was specifically higher when Y(II) was reduced (Fig. 8E). Y(NPQ) reflects nonphotochemical quenching by heat (thermal) dissipation of excitation energy in the antenna system. Y(NO), representing nonregulated energy dissipation due to PSII inactivity, Y(NPQ), and Y(II) added up to unity, and their distribution during the different treatments is given in Figure 8F. The decrease of Y(II) upon D188 infection was largely paralleled by an increase in Y(NO), indicating inhibition of photosynthesis.

The TCA cycle in the mitochondria is considered to be an integral part of the photosynthetic metabolism (Fernie et al., 2004; Nunes-Nesi et al., 2007; Noguchi and Yoshida, 2008). Among the 2-fold down-regulated genes (Table II), putative aconitases, pyruvate decarboxylases, and pyruvate phosphate dikinase, all involved in the TCA cycle, were identified. Moreover, all of the TCA cycle genes in the list of 3,422 differentially regulated genes were down-regulated at 24 dpi (Supplemental Table S2), further suggesting reduced functioning of the TCA cycle upon infection with *R. fascians* D188. This observation was partly supported by the metabolite profiles (Fig. 10). Although infection with strain D188 initially led to an accumulation of pyruvate, succinate, fumarate, and malate, at 24 dpi, when symptoms were fully established, the levels of all except succinate dropped below those measured in tissues infected with D188-5.

The bifunctional Rubisco enzyme also functions in the photorespiration process that is in competition with photosynthesis at the level of enzyme substrate (either O_2 or CO_2). In the complete differential transcript data

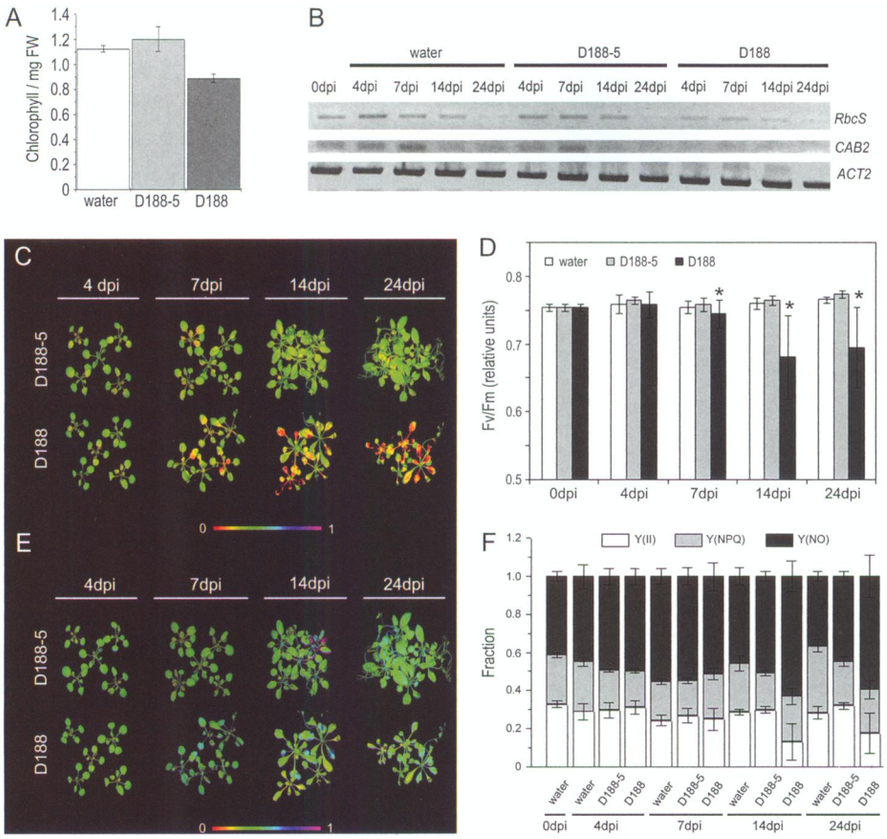

Figure 8. Decrease in photosynthesis after *R. fascians* infection. A, Chlorophyll content in plants inoculated with water, *R. fascians* D188-5, and D188 at 24 dpi. B, RT-PCR profiling of the *RbcS* and *CAB2* genes upon mock, *R. fascians* D188-5, and D188 infections. C, False-color-coded image of Y(II) upon *R. fascians* D188-5 and D188 infection at 4, 7, 14, and 24 dpi. D, F_v/F_m values upon water, *R. fascians* D188-5, and D188 infection. E, False color-coded image of q_N after *R. fascians* D188-5 and D188 infection at 4, 7, 14, and 24 dpi. F, Distribution of Y(II), Y(NPQ), and Y(NO) upon mock, *R. fascians* D188-5, and D188 infection at 4, 7, 14, and 24 dpi. Error bars represent SD ($n > 15$). Asterisks mark significant differences ($P < 0.05$). FW, Fresh weight.

set, photorespiration-related genes were initially downregulated, but at 24 dpi, the expression was activated by strain D188, suggesting that photorespiration might be enhanced (Supplemental Table S2). At the metabolite level, Gly and Ser are intermediates in the formation of glycerate that will ultimately be redirected to the chloroplasts, where it is phosphorylated to 3-phosphoglycerate to reenter the Calvin cycle. Upon infection with D188, especially at the later time points of the interaction, Gly and Ser levels were significantly lower than those of the controls (Fig. 11); in contrast, glycerate levels were up to 7-fold higher upon D188 infection, implying a flux toward this metabolite and illustrating a possible enhancement of photorespiration.

R. fascians Infection Stimulates Amino Acid and Polyamine Biosynthesis

Besides a photosynthesis-related function, the TCA cycle provides carbon skeletons for the biosynthesis of several other metabolites, such as amino acids and polyamines. The profiles of the detected amino acids indicated that the bacterial presence had a stimulating effect on the metabolic pathways, resulting in amino acid biosynthesis (Fig. 11). Nevertheless, infection with D188 generally resulted in a faster and stronger increase. The most pronounced differential accumulation was measured for Asn, Trp, Tyr, and Ala, whereas the Arg and Orn contents dropped considerably in D188-infected tissues. Interestingly, the latter are in-

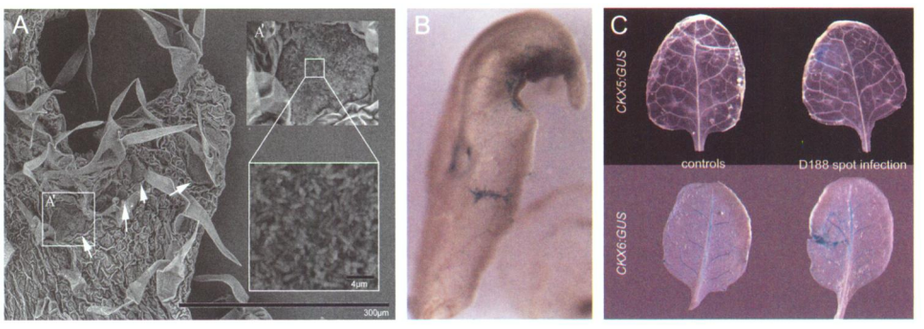

Figure 9. Colocalization of *R. fascians* microcolonies with cytokinin marker gene expression. A, Electron micrographs showing microcolonies of *R. fascians* at leaf edges. B, Symptomatic leaves of infected *ARR5:GUS* marker lines showing GUS staining at leaf edges. C, Spot inoculation of *CKX5:GUS* and *CKX6:GUS* lines with GUS staining at the inoculation sites.

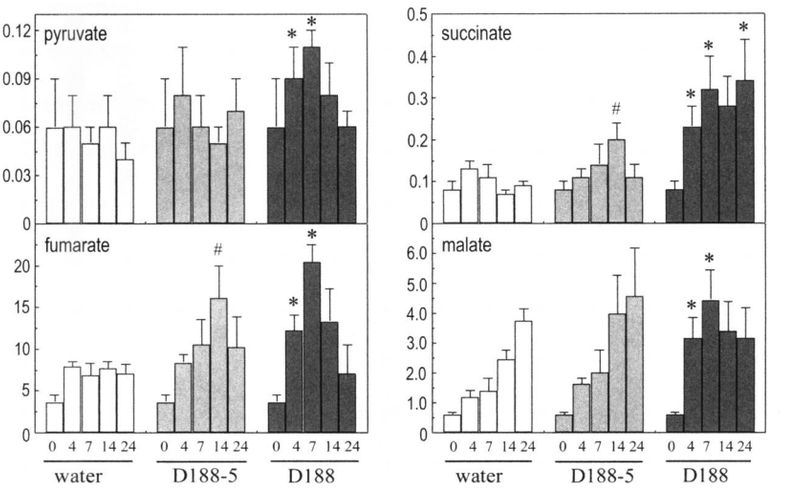

Figure 10. Responses of pyruvate and TCA cycle intermediates upon infection with *R. fascians*. Mock, *R. fascians* D188-5, and D188 infection at 4, 7, 14, and 24 dpi. Symbols (# and *) indicate statistically significant differences between D188-5 and mock samples ($P < 0.01$) and between D188-5 and D188 samples ($P < 0.01$), respectively. The metabolite abundances are expressed relative to the internal standard ribitol at each time point and normalized to the fresh weight. Error bars represent SD ($n = 6$).

termediates for polyamine biosynthesis. Indeed, putrescine levels strongly increased upon *R. fascians* D188 infection already at 4 dpi (Fig. 11).

DISCUSSION

The plant pathogenic actinomycete *R. fascians* is rather unique among the hyperplasia-inducing bacteria because it induces the formation of differentiated galls upon infection of its many hosts (Putnam and Miller, 2007). Typical symptoms observed in Arabidopsis are small serrated leaves, early flowering, inhibition of floral stalk elongation, activation of axillary meristems, de novo meristem formation in the axillary regions of the rosette, and delayed senescence. These symptoms are triggered by cytokinins secreted by the colonizing bacteria, which set off a signaling cascade leading to activation of mitotic cell divisions, prevention of endoreduplication, and ectopic expression of meristem-specific *KNOX* genes (Crespi et al., 1992, 1994; Depuydt et al., 2008, 2009). Consequently, infection results in the amplification of young tissues that do not mature. Here, we addressed the questions of how and why symptomatic tissues differ from normal tissues and how the eventual changes could contribute to the establishment of the bacterial population.

Through transcriptome analysis, we investigated the genome-wide molecular basis of symptom development. The overrepresentation of genes involved in cytokinin perception, signal transduction, and homeostasis supported the central role of these hormones in the pathology. However, the data set of genes 2-fold differentially expressed upon infection overlapped only minimally with publicly available microarray data sets that dealt with hormone treatments or biotic interactions. In other words, the *R. fascians* interaction leaves a very specific transcriptome fingerprint on Arabidopsis. The expression profiles of both up- and down-regulated genes resembled most those obtained from the interaction of *A. tumefaciens* and Arabidopsis. Interestingly, both bacteria induce galls on their host through elevated levels of cytokinins and auxins. Nevertheless, the mechanisms resulting in the hormone imbalance in the infected plant are completely different, and generally *A. tumefaciens*-induced tumors consist only of undifferentiated cells (Johnson et al., 1974).

Remarkably, the expression of genes encoding several peroxidases, a copper amino oxidase, and L-ascorbate peroxidases was significantly down-regulated upon infection with the pathogenic strain D188. These proteins are either ROS-producing or ROS-scavenging enzymes, and they play a key role in plant defense against pathogen attack by mediating an oxidative burst (Lamb and Dixon, 1997; Mittler et al., 2004). The observed down-regulation implies that during the interaction with *R. fascians* D188, no oxidative burst is initiated, which is supported by the down-regulated expression of *TRX-h5*, a marker for oxidative stress, and the reduced level of ascorbate, a major H_2O_2-scavenging antioxidant, in infected tissues. Moreover, differential accumulation of H_2O_2 could not be visualized with DAB staining and localized necrosis or cell death was not observed in Arabidopsis tissues infected with the pathogenic or the nonpathogenic *R. fascians* strains (data not shown). ROS is not only involved in structural aspects related to plant defense, such as restraining pathogen spread, modulation of plant cell wall architecture, programmed plant cell death, and the hypersensitive response (Hammond-Kosack and Jones, 1996; Dempsey et al., 1999; Torres et al., 2006) but also has a significant signaling function during these processes (Gechev et al., 2006; Torres et al., 2006). Consequently, the apparently active suppression of ROS formation by *R. fascians* possibly avoids defense onset in general. Indeed, phenolic compounds do not accumulate at the infection site (Vereecke et al., 2000; Cornelis et al., 2001), and many defense-related genes

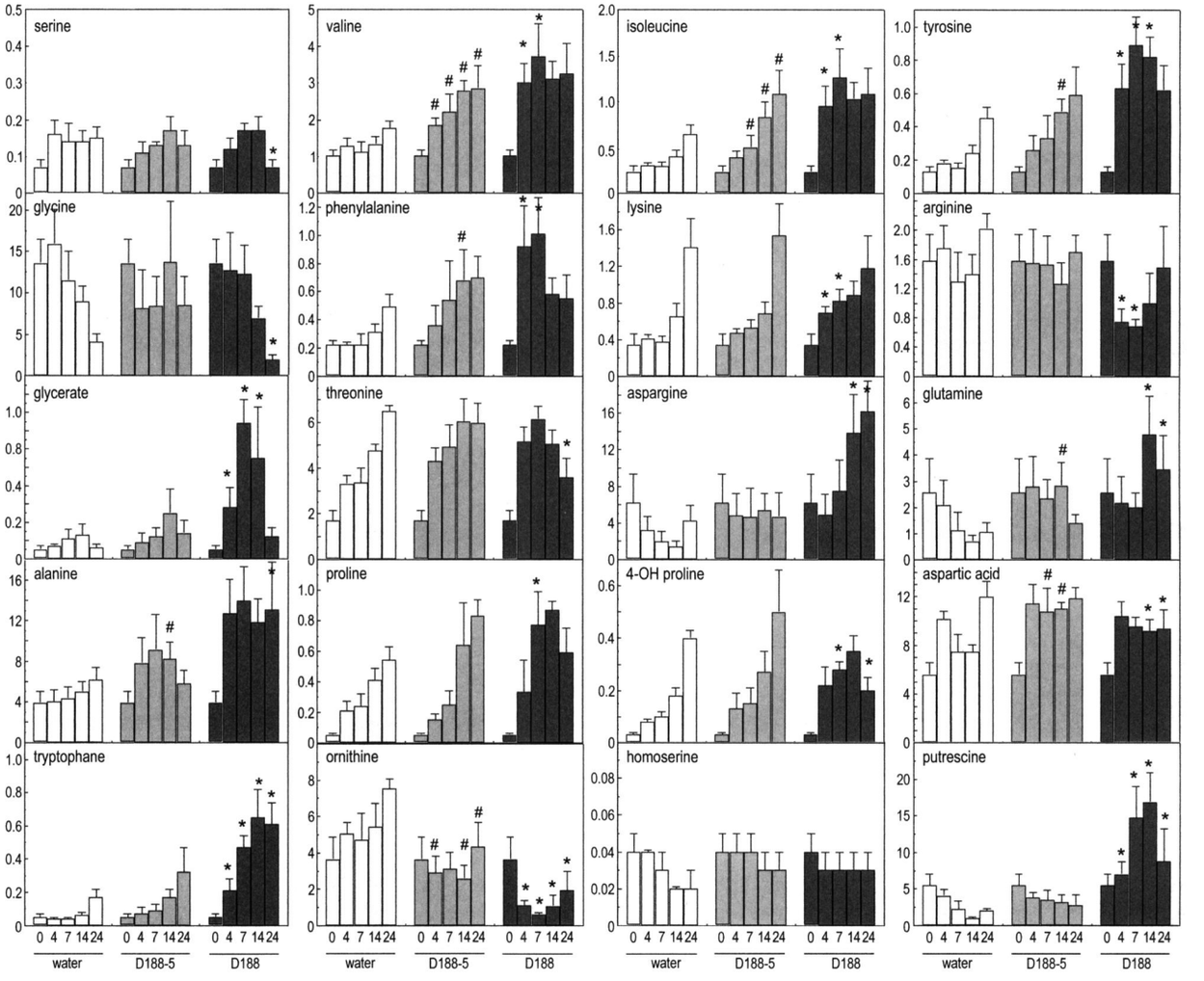

Figure 11. Effect of *R. fascians* infection on amino acids, putrescine, and glycerate levels. Mock, *R. fascians* D188-5, and D188 infection at 4, 7, 14, and 24 dpi. Symbols (# and *) indicate statistically significant changes between D188-5 and mock-infected samples ($P < 0.01$) and between D188-5 and D188 samples ($P < 0.01$), respectively. The metabolite abundances are expressed relative to the internal standard ribitol at each time point and normalized to the fresh weight. Error bars represent SD ($n = 6$).

are down-regulated upon D188 infection. Intriguingly, comparison with other data sets revealed that, while these genes were up-regulated during other biotic interactions and by cytokinin treatment, generally their expression was down-regulated during the interaction with *A. tumefaciens* and by auxin treatment. Auxin has been implicated in defense suppression, and bacterial auxin biosynthesis by *A. tumefaciens* and *P. syringae* pv *savastanoi* is crucial for repression of the hypersensitive response (Robinette and Matthysse, 1990; Navarro et al., 2004, 2006; Robert-Seilaniantz et al., 2007). Interestingly, auxins accumulate in symptomatic tissues induced by *R. fascians* (Vereecke et al., 2000; de O Manes et al., 2001) and the bacterium has been demonstrated to secrete auxins (Vandeputte et al., 2005), altogether suggesting that this bacterial morphogen might be of central importance for defense suppression.

GO annotation of the differentially expressed genes clearly pointed toward a change in the primary metabolism, a finding that was confirmed by metabolic profiling of tissues infected with *R. fascians* D188 and D188-5. A schematic overview of these metabolic changes is given in Supplemental Figure S5. Intriguingly, bacterial infection in general had a measurable impact on the primary metabolism of the plant, although the alterations induced by the pathogenic strain were much stronger. Evaluation of the carbohydrates revealed that, whereas Suc levels did not change, Glc, Fru, raffinose, maltose, and sorbose accumulated from 4 dpi onward. Importantly, upon infection, invertase transcripts and activities were

strongly enhanced, probably accounting for the observed increase in the hexose-Suc ratio and illustrating the establishment of a sink (Smeekens, 2000; Roitsch and González, 2004; Rolland et al., 2006; Berger et al., 2007). Cytokinins are known to induce invertase activity (Chou et al., 2000; Roitsch et al., 2003; Walters and McRoberts, 2006), but high sugar contents have similar effects, implying that the sink strength could be augmented by this amplified signaling. Moreover, cytokinin-induced cell wall invertase activity has been shown to increase sugar uptake by plant cells (Roitsch and Ehneß, 2000). Several genes encoding sugar transporters were indeed differentially regulated upon *R. fascians* infection (data not shown), which might contribute to the sink strength. Finally, cytokinins and sugars both control the expression of *CYCLIND3* genes, which have been shown to be instrumental for the G1-to-S transition of the cell cycle (Riou-Khamlichi et al., 2000) and for symptom development upon *R. fascians* infection (Depuydt et al., 2009). Therefore, the sink characteristics are probably correlated with symptom establishment that is an energy-demanding process, on the one hand, and with nutrition of the pathogen, on the other hand. Indeed, the accumulating carbohydrates are good carbon sources for *R. fascians* (Temmerman et al., 2000), and conversion of infected tissues into a sink has been demonstrated in several other plant-pathogen interactions (Wright et al., 1995; Chou et al., 2000; Herbers et al., 2000; Scharte et al., 2005).

Typically, source-to-sink transitions are accompanied by changes in photosynthetic capacity (Scholes et al., 1994; Chou et al., 2000; Walters and McRoberts, 2006). Gene expression data, determination of chlorophyll content, and chlorophyll fluorescence imaging altogether supported the occurrence of photosynthesis inhibition upon infection with *R. fascians*. Similarly, transcript and metabolite data indicated that the flux through the TCA cycle was also reduced when the disease became fully established, although the concentration of succinate remained high throughout the interaction and pyruvate levels were elevated at the early stages of infection. Interestingly, virulence gene expression in *R. fascians* is induced by an autoregulatory compound and the induction levels are significantly increased in the presence of succinate and pyruvate (Temmerman et al., 2000; Maes et al., 2001). The decreasing amounts of Ser and Gly, together with the increase in glycerate levels, may point to photorespiratory Gly decarboxylation that would add to the reduced photosynthetic and TCA cycle activities (Atkin et al., 2000; Raghavendra and Padmasree, 2003; Nunes-Nesi et al., 2007). Intriguingly, photorespiration had been hypothesized to play a potential role in providing specialized nutrients to the bacterium in support of endophytic colonization (Vereecke et al., 2002a, 2002b; Vandeputte et al., 2007).

Amino acid levels had generally increased during symptom development, suggesting that *R. fascians* might use them as nitrogen sources. In vitro, auxin production by the bacterium is significantly induced when excess Trp is added to the medium (Vandeputte et al., 2005). In this context, it is interesting that the augmentation of Trp was one of the highest measured. Production of the autoregulatory compound by the *att* locus involves Arg biosynthesis, and expression of the *att* genes is inhibited by Orn and Arg (Maes et al., 2001). Again, it is remarkable that the concentrations of these amino acids were lower than those of the controls at the onset of the interaction.

Orn and Arg are also precursors of polyamine biosynthesis, and the polyamine putrescine accumulates to high levels during infection. This accumulation could be interpreted as a sign of reduced catabolism; polyamine degradation has recently been described as an important source for H_2O_2 production (Walters, 2003; Cona et al., 2006; Jubault et al., 2008; Kusano et al., 2008, and refs. therein), further supporting the absence of an oxidative burst upon *R. fascians* infection. Putrescine and other polyamines have also been associated with young, metabolically active healthy and diseased tissues (Walters and Shuttleton, 1985; Galston and Sawhney, 1990). Moreover, polyamine biosynthesis is induced by cytokinins and other hormone treatments, and they are considered to be a separate class of plant hormones that control plant development (Kusano et al., 2008). The accumulation of putrescine might thus be part of the (secondary) signaling cascade that mediates symptom establishment. Similarly, trehalose, a disaccharide known as an osmoprotectant (Wingler, 2002; Penna, 2003; Luo et al., 2008), has also been attributed a signaling function in plant development (Müller et al., 2001; Vogel et al., 2001; Wingler, 2002). Trehalose concentrations in Arabidopsis are generally low through the action of trehalase. During different plant-microbe interactions, however, trehalose accumulates strongly and is believed to serve as a major carbon source for bacteria (Müller et al., 1995; Brodmann et al., 2002; Boboye, 2004; Rolland et al., 2006). Trehalose levels increased upon infection with both *R. fascians* strains, although the effect of D188 was much stronger, and interestingly, trehalose biosynthesis has been reported to be activated by cytokinin application (Brenner et al., 2005). In accordance, transcript data showed an up-regulation of *TPS1* but no differential expression of the trehalase gene.

In conclusion, the transcript and metabolite data presented here allow us to propose a model for the initiation of the interaction between *R. fascians* and Arabidopsis and the subsequent niche establishment. Epiphytic colonization triggers minor metabolic changes in the plant through the production of very low levels of morphogens and, eventually, other bacterial effectors. Importantly, early Trp accumulation might feed into the auxin biosynthetic pathway of *R. fascians*, which might down-regulate plant defense, permitting elaborate epiphytic and endophytic colonization. The metabolic modifications include a decrease in Arg and Orn and an increase in pyruvate and succinate levels, together allowing the synthesis of

the bacterial autoregulatory compound. Consequently, bacterial cytokinin biosynthesis is strongly triggered, which significantly affects the transcriptome and metabolome of the plant. Secondary signals, such as polyamines and trehalose, involved in plant development accumulate and amplify the developmental alterations that are initiated by the bacterial cytokinins. The symptomatic tissue converts into a sink through the activation of invertases, leading to an increase in carbon source levels. The simultaneous buildup of amino acids and eventually of specialized photorespiration-derived metabolites ultimately results in the establishment of a rich niche for *R. fascians*.

MATERIALS AND METHODS

Plant Material, Sampling, and Infection Conditions

Arabidopsis (*Arabidopsis thaliana* ecotype C24) was used throughout and was obtained from the European Arabidopsis Stock Centre (N906). *ARR5:GUS*, *CKX5:GUS*, and *CKX6:GUS* lines were obtained from T. Schmülling (Freie Universität Berlin). The seeds were sterilized by submergence for 2 min in 70% (v/v) ethanol, subsequently for 12 min in 5% (w/v) NaOCl supplemented with 0.1% (v/v) polyoxyethylenesorbitan 20, and rinsed at least five times with sterile water. The seeds were germinated and grown on half-strength Murashige and Skoog medium in a growth chamber under a 16-h/8-h light/dark photoperiod at 21°C ± 2°C. GUS staining was done as described previously (Depuydt et al., 2008).

The *Rhodococcus fascians* strains used were the pathogenic strain D188, containing the linear virulence plasmid pFiD188, and its plasmid-free nonpathogenic derivative D188-5 (Desomer et al., 1988). These strains were grown in liquid yeast extract broth for 2 d at 28°C under gentle agitation until late exponential phase. Prior to infection, the cultures were washed and concentrated four times by resuspending the bacterial pellets in sterile distilled water. At 16 d after germination, Arabidopsis plants were infected at the 1.05 stage (Boyes et al., 2001) by local application of a drop of bacterial culture to the shoot apical meristem. For genome-wide expression profiling, plants were sampled at 7, 14, and 24 dpi. Roots, cotyledons, and leaves were removed, yielding samples enriched in the meristematic regions, and were immediately snap frozen in liquid nitrogen. Two independent replicates of each time point-treatment combination were harvested, for a total of 12 samples. For the qRT-PCR experiments and the metabolomics analysis, complete shoots were harvested at 4, 7, 14, and 24 dpi. For spot inoculations, 5 μL of a washed bacterial culture was applied to the upper side of the leaves of *CKX5:GUS* or *CKX6:GUS* plants, incubated for 7 d, and subsequently stained for GUS activity, as described (Depuydt et al., 2008).

RNA Extraction and Labeling

RNA was extracted using the RNease Plant Mini Kit (Qiagen) according to the manufacturer's instructions. For each time point-treatment combination, RNA was extracted from a pool of 50 plants. These RNA preparations were DNase treated and purified through NH_4Ac (5 M) precipitation. Samples were quality controlled and quantified with a NanoDrop Spectrophotometer (Isogen). Samples were labeled with either Cy3 or Cy5 dye.

Hybridization and Preprocessing

Samples were hybridized to the CATMA Arabidopsis arrays (Crowe et al., 2003; Hilson et al., 2004), which are two-color arrays containing 24,576 GSTs and 384 controls. Hybridization, washing, and scanning of the arrays were carried out at the Plant Genomics Research Unit, as described previously (Lurin et al., 2004). Quality of the hybridization was assessed using control spots.

The raw expression data, comprising the logarithm of median feature pixel intensity at wavelengths 653 nm (Cy5) and 532 nm (Cy3), were uploaded into GenStat (Payne and Arnold, 2002) for further processing. The Loess procedure was applied for global intensity-dependent normalization on the log base 2 foreground intensities to correct for dye bias. No background correction was made. Each of the 14 hybridization samples was subjected to the linear mixed normalization model of the form (random effects in italics; Wolfinger et al., 2001): response = μ + *array* + *residual*, where the response variable represents the Loess-corrected $\log_2$-transformed Cy3 and Cy5 fluorescence intensity measurements of the 24,576 GSTs. Next, the estimated residuals from the normalization mixed model were subjected to a gene-specific mixed ANOVA model of the form (random effects in italics): residuals = μ + dye + treatment + time point + treatment × time point + *array* + error. The dye term models the fixed dye and replicate effects, as both effects are confounded; the array term models the effects for each spot and equals the gene × array interaction effect. Mixed models were fitted to the data by restricted maximum likelihood. Wald statistics were calculated, and significance was assigned to the interaction term treatment × time point, which identified genes that showed a differential expression pattern for both parameters (time point and treatment). An FDR was calculated for the treatment × time point interaction effect by modeling the adjusted *P* values as a two-component mixture of uniform and beta densities, as implemented in GenStat; default parameter settings were used to estimate $\pi 0$, the proportion of features that are truly null. A *P* value cutoff of 0.001 was chosen, corresponding to a FDR of 0.15% for the treatment × time point interaction effect.

All procedures comply with the MIAME (for minimum information about a microarray experiment) standards for array data (Brazma et al., 2001). The profiling data have been submitted to ArrayExpress (accession no. E-MEXP-1893).

RT-PCR Primers and Conditions

For qRT-PCR analysis, 2 μg of RNA was reverse transcribed into cDNA synthesis with the SuperScript Reverse Transcriptase Kit (Invitrogen), subsequently diluted 50 times, and stored at −20°C until further use. RT-PCR was done on cDNA derived from complete shoot material to investigate invertase and photosynthetic gene expression. The cell wall (*FRUCT1* and *FRUCT2*) and vacuolar (*FRUCT3* and *FRUCT4*) invertases were amplified in 25 cycles with primers described by Tymowska-Lalanne and Kreis (1998). The expression profile of the cytoplasmic/neutral invertases was examined with primers developed by Vargas et al. (2008) in 22 amplification cycles. The *RbcS* primer set was obtained from Laval et al. (2002), and *CAB2* was amplified with primers described by Delessert et al. (2004), both in 18 amplification cycles.

Metabolomics Analysis

The primary metabolite profiles of complete shoots of mock-inoculated controls and plants infected with *R. fascians* D188-5 and D188 were compared in six independent biological replicates at 0, 4, 7, 14, and 24 dpi. To extract soluble metabolites for GC-MS analysis, 100 mg of ground shoot material was extracted in 1.4 mL of 100% (v/v) methanol together with 60 μL of an internal standard (0.2% [w/v] ribitol in water). The mixture was heated for 15 min at 70°C with vigorous mixing. After centrifugation, 750 μL of chloroform and 1.5 mL of water were added to the supernatant and vortexed for 30 s. The phases were separated by centrifugation, and aliquots of the methanol/water phase (containing the polar metabolites) were taken and reduced to dryness in a SpeedVac concentrator. Samples were dissolved in 40 μL of 20 mg mL^{-1} methoxyamine hydrochloride in pyridine for 2 h at 37°C to protect the carbonyl moieties. Next, 10 μL of a retention time standard mixture (0.029% [v/v] *n*-dodecane, *n*-pentadecane, *n*-nonadecane, *n*-docosane, *n*-octacosane, *n*-dotracontane, and *n*-hexatriacontane dissolved in pyridine) was added. Acidic protons were derivatized by treatment with 70 μL of *N*-methyl-*N*-(trimethylsilyl)trifluoracetamide for 30 min at 37°C. The GC-MS profiling method was largely as described previously (Lisec et al., 2006). Samples in each batch were analyzed in random order. GC-MS spectra were obtained with an AS 2000 autosampler and a GC8000 gas chromatograph coupled to a Thermo Finnigan Voyager quadrupole-type mass spectrometer, operated by MassLab software (ThermoQuest; Thermo Fisher Life Scientific). GC-MS hardware, settings, and data analysis were as described (Lisec et al., 2006; Schauer et al., 2006).

Chlorophyll Fluorescence Imaging

Chlorophyll fluorescence parameters were measured with an Imaging-PAM Chlorophyll Fluorometer (Walz). Mock-inoculated controls and *R. fascians*-infected plants (strains D188 and D188-5) were compared in their photosynthetic capacity at 4, 7, 14, and 21 dpi. At least 15 areas of interest, over

which the values of the selected fluorescence parameters were averaged, were marked for each condition of each parameter, and their average was used for downstream analysis. With the Imaging-PAM, the current fluorescence yield (F_t) was continuously measured. After determining the dark-level fluorescence yield ($F_t = F_0$), for which the plants were dark adapted for 15 min, an 800-ms saturating pulse was applied to determine the maximum fluorescence (F_m). The maximum quantum yield of PSII photochemistry, $F_v/F_m = (F_m - F_0)/F_m$, was then automatically calculated by the ImagingWin software (Walz). In the presence of actinic illumination, the current fluorescence yield ($F_t = F$) and the maximum light-adapted fluorescence (F_m') were determined, from which the effective PSII quantum yield [Y(II) = $(F_m' - F_t)/F_m'$] was automatically derived. The coefficient of nonphotochemical quenching, qN = $(F_m - F_m')/(F_m' - F_0')$, with F_0' estimated according to Oxborough and Baker (1997), was calculated by the ImagingWin software, as were the parameters of the effective PSII quantum yields of regulated nonphotochemical energy dissipation, Y(NPQ), and nonregulated energy dissipation, Y(NO), which are complementary with the photochemical quantum yield [i.e. Y(II) + Y(NPQ) + Y(NO) = 1]. Y(II) represents the proportion of absorbed light that is used for photosynthetic electron transport through PSII and is thus essentially the operating efficiency of PSII measured in the light. F_v/F_m is the maximum efficiency of PSII and is a useful measure for photoinhibition, and Y(NPQ) describes the efficiency with which energy is dissipated nonphotochemically as heat. Images of the fluorescence parameters were displayed with the help of a false-color code ranging from 0 (black) to 1 (purple) as implemented in the ImagingWin software.

Scanning Electron Microscopy

The samples were analyzed by scanning electron microscopy with a tabletop microscope TM-1000 (Hitachi) without sample processing. Images were taken with the accompanying software.

Invertase Activity Tests

To assay the activities of the cytosolic, vacuolar, and cell wall invertases, the extraction was carried out as described (Wright et al., 1998), with approximately 150 mg of ground shoot tissue of each infection condition supplemented with 1.2 mL of extraction buffer (50 mM HEPES-KOH, pH 8.0, 5 mM $MgCl_2$, 2 mM EDTA, 1 mM $CaCl_2$, 1 mM benzamidine, 1 mM dithiothreitol, and 0.1 mM phenylmethylsulfonyl fluoride). The mixture was incubated on ice for 10 min. After centrifugation (13,000*g*, 10 min, 4°C), the supernatant (containing cytosolic and vacuolar invertases) was transferred to a new tube. For determination of cell wall invertase activities, the pellet was washed three times and finally resuspended in 1.2 mL of extraction buffer. Extracts were used without dialysis. The invertase reactions were carried out in 0.08 M citrate/phosphate buffers with 0.1 M Suc as a substrate at pH 4.5, 5.5, and 7.5 for cell wall, vacuolar, and cytoplasmic invertases, respectively (Scholes et al., 1994). Of the extracts, 100 μL was added to the reaction mixtures in a final volume of 300 μL. After 45 min of incubation at 37°C, the reaction was stopped by adding 0.1 mL of 1 M Tris-HCl and incubated for 4 min at 95°C. The amounts of Glc and Fru liberated in the reaction were determined by an enzyme-linked assay (Scholes et al., 1994): 30 μL of the invertase reaction was added to 200 μL of a buffer cocktail (1 M imidazole-HCl, pH 6.9, 2 M $MgCl_2$, 100 mM NADP, 100 mM ATP, and 400 units mL^{-1} Glc-6-P dehydrogenase) on a multiwell plate. Next, 5 μL of hexokinase (300 units mL^{-1}) was added, and the minimum and maximum absorbance were recorded at 340 nm. Subsequently, 5 μL of phosphoglucoisomerase (140 units mL^{-1}) was added, and the minimum and maximum optical densities were recorded to calculate the enzymatic activity of the samples. Each reaction was done in triplicate.

Supplemental Data

The following materials are available in the online version of this article.

Supplemental Figure S1. qRT-PCR confirmation of 10 differentially expressed genes randomly taken from the microarray data set.

Supplemental Figure S2. BiNGO analysis of all up-regulated genes throughout *R. fascians* infection.

Supplemental Figure S3. BiNGO analysis of all down-regulated genes throughout *R. fascians* infection.

Supplemental Figure S4. Effect of *R. fascians* infection on ascorbate and dehydroascorbate levels.

Supplemental Figure S5. Overview of significant changes in the primary metabolism upon infection with *R. fascians* D188 when compared with D188-5 infection.

Supplemental Table S1. Differential expression of putative defense genes upon *R. fascians* D188 infection.

Supplemental Table S2. TCA cycle and photorespiration genes differentially expressed upon *R. fascians* D188 infection.

ACKNOWLEDGMENTS

We thank Koen Goethals and Rosemary Loria for fruitful discussions, Thomas Schmülling for *ARR5:GUS*, *CKX5:GUS*, and *CKX6:GUS* seeds, Elisabeth Stes for DAB staining, Annick De Keyser for technical assistance, and Martine De Cock for help in preparing the manuscript.

Received October 28, 2008; accepted December 25, 2008; published December 31, 2008.

LITERATURE CITED

Atkin OK, Millar AH, Gardeström P, Day DA (2000) Photosynthesis, carbohydrate metabolism and respiration in leaves of higher plants. *In* RC Leegood, TD Sharkey, S von Caemmerer, eds, Photosynthesis: Physiology and Metabolism, Advances in Phytosynthesis and Respiration, Vol 9. Kluwer Academic Publishers, Dordrecht, The Netherlands, pp 153–175

Berger S, Papadopoulos M, Schreiber U, Kaiser W, Roitsch T (2004) Complex regulation of gene expression, photosynthesis and sugar levels by pathogen infection in tomato. Physiol Plant **122:** 419–428

Berger S, Sinha AK, Roitsch T (2007) Plant physiology meets phytopathology: plant primary metabolism and plant-pathogen interactions. J Exp Bot **58:** 4019–4026

Biemelt S, Sonnewald U (2006) Plant-microbe interactions to probe regulation of plant carbon metabolism. J Plant Physiol **163:** 307–318

Boboye B (2004) Degradation of trehalose by rhizobia and characteristics of a trehalose-degrading enzyme isolated from *Rhizobium* species NGR234. J Appl Microbiol **97:** 256–261

Boyes DC, Zayed AM, Ascenzi R, McCaskill AJ, Hoffman NE, Davis KR, Görlach J (2001) Growth stage-based phenotypic analysis of *Arabidopsis*: a model for high throughput functional genomics in plants. Plant Cell **13:** 1499–1510

Brazma A, Hingamp P, Quackenbusch J, Sherlock G, Spellman P, Stoeckert C, Aach J, Ansorge W, Ball CA, Causton HC, et al (2001) Minimum information about a microarray experiment (MIAME): toward standards for microarray data. Nat Genet **29:** 365–371

Brenner WG, Romanov GA, Köllmer I, Bürkle L, Schmülling T (2005) Immediate-early and delayed cytokinin response genes of *Arabidopsis thaliana* identified by genome-wide expression profiling reveal novel cytokinin-sensitive processes and suggest cytokinin action through transcriptional cascades. Plant J **44:** 314–333

Brodmann D, Schuller A, Ludwig-Müller J, Aeschbacher RA, Wiemken A, Boller T, Wingler A (2002) Induction of trehalase in *Arabidopsis* plants infected with the trehalose-producing pathogen *Plasmodiophora brassicae*. Mol Plant Microbe Interact **15:** 693–700

Chou H-M, Bundock N, Rolfe SA, Scholes JD (2000) Infection of *Arabidopsis thaliana* leaves with *Albugo candida* (white blister rust) causes a reprogramming of host metabolism. Mol Plant Pathol **1:** 99–113

Cona A, Rea G, Angelini R, Federico R, Tavladoraki P (2006) Functions of amine oxidases in plant development and defence. Trends Plant Sci **11:** 80–88

Cornelis K, Maes T, Jaziri M, Holsters M, Goethals K (2002) Virulence genes of the phytopathogen *Rhodococcus fascians* show specific spatial and temporal expression patterns during plant infection. Mol Plant Microbe Interact **15:** 398–403

Cornelis K, Ritsema T, Nijsse J, Holsters M, Goethals K, Jaziri M (2001) The plant pathogen *Rhodococcus fascians* colonizes the exterior and interior of the aerial parts of plants. Mol Plant Microbe Interact **14:** 599–608

Crespi M, Messens E, Caplan AB, Van Montagu M, Desomer J (1992) Fasciation induction by the phytopathogen *Rhodococcus fascians* depends upon a linear plasmid encoding a cytokinin synthase gene. EMBO J **11:** 795–804

Crespi M, Vereecke D, Temmerman W, Van Montagu M, Desomer J (1994) The *fas* operon of *Rhodococcus fascians* encodes new genes required for efficient fasciation of host plants. J Bacteriol **176:** 2492–2501

Crowe ML, Serizet C, Thareau V, Aubourg S, Rouzé P, Hilson P, Beynon J, Weisbeek P, Van Hummelen P, Reymond P, et al (2003) CATMA: a complete *Arabidopsis* GST database. Nucleic Acids Res **31:** 156–158

D'Agostino IB, Deruère J, Kieber JJ (2000) Characterization of the response of the Arabidopsis response regulator gene family to cytokinin. Plant Physiol **124:** 1706–1717

Delessert C, Wilson IW, Van Der Straeten D, Dennis ES, Dolferus R (2004) Spatial and temporal analysis of the local response to wounding in *Arabidopsis* leaves. Plant Mol Biol **55:** 165–181

Dempsey DA, Shah J, Klessig DF (1999) Salicylic acid and disease resistance in plants. Crit Rev Plant Sci **18:** 547–575

de O Manes C-L, Beeckman T, Ritsema T, Van Montagu M, Goethals K, Holsters M (2004) Phenotypic alterations in *Arabidopsis thaliana* plants caused by *Rhodococcus fascians* infection. J Plant Res **117:** 139–145

de O Manes C-L, Van Montagu M, Prinsen E, Goethals K, Holsters M (2001) De novo cortical cell division triggered by the phytopathogen *Rhodococcus fascians* in tobacco. Mol Plant Microbe Interact **14:** 189–195

Depuydt S, De Veylder L, Holsters M, Vereecke D (2009) Eternal youth, the fate of developing Arabidopsis leaves upon *Rhodococcus fascians* infection. Plant Physiol **149:** 1387–1398

Depuydt S, Doležal K, Van Lijsebettens M, Moritz T, Holsters M, Vereecke D (2008) Modulation of the hormone setting by *Rhodococcus fascians* results in ectopic *KNOX* activation in Arabidopsis. Plant Physiol **146:** 1267–1281

Desomer J, Dhaese P, Van Montagu M (1988) Conjugative transfer of cadmium resistance plasmids in *Rhodococcus fascians* strains. J Bacteriol **170:** 2401–2405

Doehlemann G, Wahl R, Vranes M, de Vries RP, Kämper J, Kahmann R (2008) Establishment of compatibility in the *Ustilago maydis*/maize pathosystem. J Plant Physiol **165:** 29–40

Downes BP, Crowell DN (1998) Cytokinin regulates the expression of a soybean β-expansin gene by a post-transcriptional mechanism. Plant Mol Biol **37:** 437–444

Ehness R, Ecker M, Godt DE, Roitsch T (1997) Glucose and stress independently regulate source and sink metabolism and defense mechanisms via signal transduction pathways involving protein phosphorylation. Plant Cell **9:** 1825–1841

Essmann J, Schmitz-Thom I, Schön H, Sonnewald S, Weis E, Scharte J (2008) RNA interference-mediated repression of cell wall invertase impairs defense in source leaves of tobacco. Plant Physiol **147:** 1288–1299

Fernie AR, Carrari F, Sweetlove LJ (2004) Respiratory metabolism: glycolysis, the TCA cycle and mitochondrial electron transport. Curr Opin Plant Biol **7:** 254–261

Gadjev I, Vanderauwera S, Gechev TS, Laloi C, Minkov IN, Shulaev V, Apel K, Inzé D, Mittler R, Van Breusegem F (2006) Transcriptomic footprints disclose specificity of reactive oxygen species signaling in Arabidopsis. Plant Physiol **141:** 436–445

Galston AW, Sawhney RK (1990) Polyamines in plant physiology. Plant Physiol **94:** 406–410

Garcia-Brugger A, Lamotte O, Vandelle E, Bourque S, Lecourieux D, Poinssot B, Wendehenne D, Pugin A (2006) Early signaling events induced by elicitors of plant defenses. Mol Plant Microbe Interact **19:** 711–724

Gartemann K-H, Abt B, Bekel T, Burger A, Engemann J, Flügel M, Gaigalat L, Goesmann A, Gräfen I, Kalinowski J, et al (2008) The genome sequence of the tomato-pathogenic actinomycete *Clavibacter michiganensis* subsp. *michiganensis* NCPPB382 reveals a large island involved in pathogenicity. J Bacteriol **190:** 2138–2149

Gechev TS, Van Breusegem F, Stone JM, Denev I, Laloi C (2006) Reactive oxygen species as signals that modulate plant stress responses and programmed cell death. Bioessays **28:** 1091–1101

Goethals K, Vereecke D, Jaziri M, Van Montagu M, Holsters M (2001) Leafy gall formation by *Rhodococcus fascians*. Annu Rev Phytopathol **39:** 27–52

Hammond-Kosack KE, Jones JDG (1996) Resistance gene-dependent plant defense responses. Plant Cell **8:** 1773–1791

Herbers K, Meuwly P, Frommer WB, Métraux J-P, Sonnewald U (1996) Systemic acquired resistance mediated by the ectopic expression of invertase: possible hexose sensing in the secretory pathway. Plant Cell **8:** 793–803

Herbers K, Sonnewald U (1998) Molecular determinants of sink strength. Curr Opin Plant Biol **1:** 207–216

Herbers K, Takahata Y, Melzer M, Mock H-P, Hajirezaei M, Sonnewald U (2000) Regulation of carbohydrate partitioning during the interaction of potato virus Y with tobacco. Mol Plant Pathol **1:** 51–59

Hilson P, Allemeersch J, Altmann T, Aubourg S, Avon A, Beynon J, Bhalerao RP, Bitton F, Caboche M, Cannoot B, et al (2004) Versatile gene-specific sequence tags for *Arabidopsis* functional genomics: transcript profiling and reverse genetics applications. Genome Res **14:** 2176–2189

Jameson P (2000) Cytokinins and auxins in plant-pathogen interactions—an overview. Plant Growth Regul **32:** 369–380

Johnson R, Guderian RH, Eden F, Chilton M-D, Gordon MP, Nester EW (1974) Detection and quantitation of octopine in normal plant tissue and in crown gall tumors. Proc Natl Acad Sci USA **71:** 536–539

Jones JDG, Dangl JL (2006) The plant immune system. Nature **444:** 323–329

Jubault M, Hamon C, Gravot A, Lariagon C, Delourme R, Bouchereau A, Manzanares-Dauleux MJ (2008) Differential regulation of root arginine catabolism and polyamine metabolism in clubroot-susceptible and partially resistant Arabidopsis genotypes. Plant Physiol **146:** 2008–2019

Jwa N-S, Agrawal GK, Tamogami S, Yonekura M, Han O, Iwahashi H, Rakwal R (2006) Role of defense/stress-related marker genes, proteins and secondary metabolites in defining rice self-defense mechanisms. Plant Physiol Biochem **44:** 261–273

Kocal N, Sonnewald U, Sonnewald S (2008) Cell wall-bound invertase limits sucrose export and is involved in symptom development and inhibition of photosynthesis during compatible interaction between tomato and *Xanthomonas campestris* pv *vesicatoria*. Plant Physiol **148:** 1523–1536

Korves TM, Bergelson J (2003) A developmental response to pathogen infection in Arabidopsis. Plant Physiol **133:** 339–347

Kusano T, Berberich T, Tateda C, Takahashi Y (2008) Polyamines: essential factors for growth and survival. Planta **228:** 367–381

Laloi C, Mestres-Ortega D, Marco Y, Meyer Y, Reichheld J-P (2004) The Arabidopsis cytosolic thioredoxin *h5* gene induction by oxidative stress and its W-box-mediated response to pathogen elicitor. Plant Physiol **134:** 1006–1016

Lamb C, Dixon RA (1997) The oxidative burst in plant disease resistance. Annu Rev Plant Physiol Plant Mol Biol **48:** 251–275

Laval V, Koroleva OA, Murphy E, Lu C, Milner JJ, Hooks MA, Tomos AD (2002) Distribution of actin gene isoforms in the *Arabidopsis* leaf measured in microsamples from intact individual cells. Planta **215:** 287–292

Lisec J, Schauer N, Kopka J, Willmitzer L, Fernie AR (2006) Gas chromatography mass spectrometry-based metabolite profiling in plants. Nat Protoc **1:** 387–396

Loria R, Kers J, Joshi M (2006) Evolution of plant pathogenicity in *Streptomyces*. Annu Rev Phytopathol **44:** 467–487

Luo Y, Li W-M, Wang W (2008) Trehalose: protector of antioxidant enzymes or reactive oxygen species scavenger under heat stress? Environ Exp Bot **63:** 378–384

Lurin C, Andrés C, Aubourg S, Bellaoui M, Bitton F, Bruyère C, Caboche M, Debast C, Gualberto J, Hoffmann B, et al (2004) Genome-wide analysis of *Arabidopsis* pentatricopeptide repeat proteins reveals their essential role in organelle biogenesis. Plant Cell **16:** 2089–2103

Maere S, Heymans K, Kuiper M (2005) *BiNGO*: a Cytoscape plugin to assess enrichment of Gene Ontology categories in Biological Networks. Bioinformatics **21:** 3448–3449

Maes T, Vereecke D, Ritsema T, Cornelis K, Ngo Thi Thu H, Van Montagu M, Holsters M, Goethals K (2001) The *att* locus of *Rhodococcus fascians* strain D188 is essential for full virulence on tobacco through the production of an autoregulatory compound. Mol Microbiol **42:** 13–28

Maxwell K, Johnson GN (2000) Chlorophyll fluorescence—a practical guide. J Exp Bot **51:** 659–668

Mittler R, Vanderauwera S, Gollery M, Van Breusegem F (2004) The reactive oxygen gene network in plants. Trends Plant Sci **9:** 490–498

Miyawaki K, Matsumoto-Kitano M, Kakimoto T (2004) Expression of cytokinin biosynthetic isopentenyltransferase genes in *Arabidopsis*: tissue specificity and regulation by auxin, cytokinin, and nitrate. Plant J **37:** 128–138

Mogensen JE, Wimmer R, Larsen JN, Spangfort MD, Otzen DE (2002) The major birch allergen, Bet v 1, shows affinity for a broad spectrum of physiological ligands. J Biol Chem **277:** 23684–23692

Müller J, Aeschbacher RA, Wingler A, Boller T, Wiemken A (2001) Trehalose and trehalase in Arabidopsis. Plant Physiol **125:** 1086–1093

Müller J, Boller T, Wiemken A (1995) Trehalose and trehalase in plants: recent developments. Plant Sci **112:** 1–9

Murgia I, Briat JF, Tarantino D, Soave C (2001) Plant ferritin accumulates in response to photoinhibition but its ectopic overexpression does not protect against photoinhibition. Plant Physiol Biochem **39:** 797–805

Navarro L, Dunoyer P, Jay F, Arnold B, Dharmasiri N, Estelle M, Voinnet O, Jones JDG (2006) A plant miRNA contributes to antibacterial resistance by repressing auxin signaling. Science **312:** 436–439

Navarro L, Zipfel C, Rowland O, Keller I, Robatzek S, Boller T, Jones JDG (2004) The transcriptional innate immune response to flg22: interplay and overlap with Avr gene-dependent defense responses and bacterial pathogenesis. Plant Physiol **135:** 1113–1128

Nielsen TH, Krapp A, Röper-Schwarz U, Stitt M (1998) The sugar-mediated regulation of genes encoding the small subunit of Rubisco and the regulatory subunit of ADP glucose pyrophosphorylase is modified by phosphate and nitrogen. Plant Cell Environ **21:** 443–454

Noguchi K, Yoshida K (2008) Interaction between photosynthesis and respiration in illuminated leaves. Mitochondrion **8:** 87–99

Nunes-Nesi A, Sweetlove LJ, Fernie AR (2007) Operation and function of the tricarboxylic acid cycle in the illuminated leaf. Physiol Plant **129:** 45–56

Oxborough K, Baker NR (1997) An instrument capable of imaging chlorophyll *a* fluorescence from intact leaves at very low irradiance and at cellular and subcellular levels of organization. Plant Cell Environ **20:** 1473–1483

Payne RW, Arnold GM (2002) GenStat Release 6.1 Reference Manual Part 3: Procedure Library PL14. VSN International, Hemel Hempstead, UK

Penna S (2003) Building stress tolerance through over-producing trehalose in transgenic plants. Trends Plant Sci **8:** 355–357

Pertry I, Václavíková K, Depuydt S, Galuszka P, Spíchal L, Temmerman W, Stes E, Schmülling T, Kakimoto T, Van Montagu M, et al (2009) Identification of *Rhodococcus fascians* cytokinins and their modus operandi to reshape the plant. Proc Natl Acad Sci USA **106:** 929–934

Putnam ML, Miller ML (2007) *Rhodococcus fascians* in herbaceous perennials. Plant Dis **91:** 1064–1076

Quilliam RS, Swarbrick PJ, Scholes JD, Rolfe SA (2006) Imaging photosynthesis in wounded leaves of *Arabidopsis thaliana*. J Exp Bot **57:** 55–69

Raghavendra AS, Padmasree K (2003) Beneficial interactions of mitochondrial metabolism with photosynthetic carbon assimilation. Trends Plant Sci **8:** 546–553

Rashotte AM, Carson SDB, To JPC, Kieber JJ (2003) Expression profiling of cytokinin action in Arabidopsis. Plant Physiol **132:** 1998–2011

Riou-Khamlichi C, Menges M, Healy JMS, Murray JAH (2000) Sugar control of the plant cell cycle: differential regulation of *Arabidopsis* D-type cyclin gene expression. Mol Cell Biol **20:** 4513–4521

Robert-Seilaniantz A, Navarro L, Bari R, Jones JDG (2007) Pathological hormone imbalances. Curr Opin Plant Biol **10:** 372–379

Robinette D, Matthysse AG (1990) Inhibition by *Agrobacterium tumefaciens* and *Pseudomonas savastanoi* of development of the hypersensitive response elicited by *Pseudomonas syringae* pv. *phaseolicola*. J Bacteriol **172:** 5742–5749

Roitsch T (1999) Source-sink regulation by sugar and stress. Curr Opin Plant Biol **2:** 198–206

Roitsch T, Balibrea ME, Hofmann M, Proels R, Sinha AK (2003) Extracellular invertase: key metabolic enzyme and PR protein. J Exp Bot **54:** 513–524

Roitsch T, Ehneß R (2000) Regulation of source/sink relations by cytokinins. Plant Growth Regul **32:** 359–367

Roitsch T, González M-C (2004) Function and regulation of plant invertases: sweet sensations. Trends Plant Sci **9:** 606–613

Rolland F, Baena-Gonzalez E, Sheen J (2006) Sugar sensing and signaling in plants: conserved and novel mechanisms. Annu Rev Plant Biol **57:** 675–709

Salvucci ME (2008) Association of Rubisco activase with chaperonin-60β: a possible mechanism for protecting photosynthesis during heat stress. J Exp Bot **59:** 1923–1933

Scharte J, Schön H, Weis E (2005) Photosynthesis and carbohydrate metabolism in tobacco leaves during an incompatible interaction with *Phytophthora nicotianae*. Plant Cell Environ **28:** 1421–1435

Schauer N, Semel Y, Roessner U, Gur A, Balbo I, Carrari F, Pleban T, Perez-Melis A, Bruedigam C, Kopka J, et al (2006) Comprehensive metabolic profiling and phenotyping of interspecific introgression lines for tomato improvement. Nat Biotechnol **24:** 447–454

Scholes JD, Lee PJ, Horton P, Lewis DH (1994) Invertase: understanding changes in the photosynthetic and carbohydrate metabolism of barley leaves infected with powdery mildew. New Phytol **126:** 213–222

Simón-Mateo C, Depuydt S, de Oliveira Manes CL, Cnudde F, Holsters M, Goethals K, Vereecke D (2006) The phytopathogen *Rhodococcus fascians* breaks apical dominance and activates axillary meristems by inducing plant genes involved in hormone metabolism. Mol Plant Pathol **7:** 103–112

Smeekens S (2000) Sugar-induced signal transduction in plants. Annu Rev Plant Physiol Plant Mol Biol **51:** 49–81

Swarbrick PJ, Schulze-Lefert P, Scholes J (2006) Metabolic consequences of susceptibility and resistance (race-specific and broad-spectrum) in barley leaves challenged with powdery mildew. Plant Cell Environ **29:** 1061–1076

Temmerman W, Vereecke D, Dreesen R, Van Montagu M, Holsters M, Goethals K (2000) Leafy gall formation is controlled by *fasR*, an AraC-type regulatory gene, in *Rhodococcus fascians*. J Bacteriol **182:** 5832–5840

Torres MA, Jones JDG, Dangl JL (2006) Reactive oxygen species signaling in response to pathogens. Plant Physiol **141:** 373–378

Truman W, Torres de Zabala M, Grant M (2006) Type III effectors orchestrate a complex interplay between transcriptional networks to modify basal defence responses during pathogenesis and resistance. Plant J **46:** 14–33

Tymowska-Lalanne Z, Kreis M (1998) Expression of the *Arabidopsis thaliana* invertase gene family. Planta **207:** 259–265

Vandeputte O, Öden S, Mol A, Vereecke D, Goethals K, El Jaziri M, Prinsen E (2005) Biosynthesis of auxin by the Gram-positive phytopathogen *Rhodococcus fascians* is controlled by compounds specific to infected plant tissues. Appl Environ Microbiol **71:** 1169–1177

Vandeputte O, Vereecke D, Mol A, Lenjou M, Van Bockstaele D, El Jaziri M, Baucher M (2007) *Rhodococcus fascians* infection accelerates progression of tobacco BY-2 cells into mitosis through rapid changes in plant gene expression. New Phytol **175:** 140–154

Vargas WA, Pontis HG, Salerno GL (2008) New insights on sucrose metabolism: evidence for an active A/N-Inv in chloroplasts uncovers a novel component of the intracellular carbon trafficking. Planta **227:** 795–807

Vereecke D, Burssens S, Simón-Mateo C, Inzé D, Van Montagu M, Goethals K, Jaziri M (2000) The *Rhodococcus fascians*-plant interaction: morphological traits and biotechnological applications. Planta **210:** 241–251

Vereecke D, Cornelis K, Temmerman W, Holsters M, Goethals K (2002a) Versatile persistence pathways for pathogens of animals and plants. Trends Microbiol **10:** 485–488

Vereecke D, Cornelis K, Temmerman W, Jaziri M, Van Montagu M, Holsters M, Goethals K (2002b) Chromosomal locus that affects the pathogenicity of *Rhodococcus fascians*. J Bacteriol **184:** 1112–1120

Vogel G, Fiehn O, Jean-Richard-dit-Bressel L, Boller T, Wiemken A, Aeschbacher RA, Wingler A (2001) Trehalose metabolism in *Arabidopsis*: occurrence of trehalose and molecular cloning and characterization of trehalose-6-phosphate synthase homologues. J Exp Bot **52:** 1817–1826

Walters DR (2003) Polyamines and plant disease. Phytochemistry **64:** 97–107

Walters DR, McRoberts N (2006) Plants and biotrophs: a pivotal role for cytokinins? Trends Plant Sci **11:** 581–586

Walters DR, Shuttleton MA (1985) Polyamines in the roots of turnip infected with *Plasmodiophora brassicae* Wor. New Phytol **100:** 209–214

Wingler A (2002) The function of trehalose biosynthesis in plants. Phytochemistry **60:** 437–440

Wolfinger RD, Gibson G, Wolfinger ED, Bennett L, Hamadeh H, Bushel P, Afshari C, Paules RS (2001) Assessing gene significance from cDNA microarray expression data via mixed models. J Comput Biol **8:** 625–637

Wright DP, Baldwin BC, Shephard MC, Scholes JD (1995) Source-sink relationships in wheat leaves infected with powdery mildew. I. Alterations in carbohydrate metabolism. Physiol Mol Plant Pathol **47:** 237–253

Wright DP, Read DJ, Scholes JD (1998) Mycorrhizal sink strength influences whole plant carbon balance of *Trifolium repens* L. Plant Cell Environ **21:** 881–891

Zimmermann P, Hirsch-Hoffmann M, Hennig L, Gruissem W (2004) GENEVESTIGATOR: Arabidopsis microarray database and analysis toolbox. Plant Physiol **136:** 2621–2632